International Journal of Scientific Research and Engineering Development-– Volume 4 Issue 3, May June 2021

Available at www.ijsred.com

RESEARCH ARTICLE OPEN ACCESS

Structural Interpretation and Hydrocarbon Prospectivity of Eastern Cordillera (Onshore Colombia) Fault and Thrust Belt

Sadiq Muhammad Rijiya*

*(Earth Science and Engineering, Imperial College London, England)

Email: sadiq.rijiya18@alumni.imperial.ac.uk

----------**********----------

Abstract:

Structural interpretation and hydrocarbon prospectivity of the Eastern Cordillera was carried out using potential field data (gravity and magnetotelluric) aided with seismic and geological cross sections. Survey and public domains gravity data were used to conduct a regional qualitative interpretation aimed at understanding the distribution of sedimentary basins and complex structural framework. A regional NE – SW trend and five structural domains which include the Eastern and Western Foothills, the Eastern and Western Inverted Domains (anticlinoria) and a Central Depressional Domain were mapped and confirmed with existing literature. To further quantify the results obtained from the qualitative interpretations, 2D forward modeling was carried out on 28 cross sections focusing mainly on the thrust regime. Regional depth surface of the Moho and a Shuttle Radar Topographic Mission (SRTM) altitude map of the study area were integrated into the model to estimate crustal thickness and topographic horizon. The models consist of four units which are the Moho, Paleozoic Basement, Cretaceous and the Cenozoic with corresponding gravity values of 3.3 g/cc, 2.7 g/cc, 2.5 g/cc and 2.4 g/cc respectively. An initial model was built to honor interpretation of cross sections followed by sensitivity tests to produce a calculated forward model. Constrained with response of the gravity data, modifications to the initial interpretations were conducted to produce an end member model that honors all available datasets in a geologically realistic manner. Depth surfaces of the Top Basement, Top Cretaceous and Top Cenozoic were generated from the 2D forward models and used as input to build a 3D gravity inversion model. Isopach map from the 3D inversion shows a sediment thickness up to 8.5 km within the sediment rich areas. Depth cross sections taken from the 3D results indicate the presence of four-way and 3-way dip closures; potential traps for hydrocarbon prospection.

Keywords **—Structural Geology, Basin Analysis, Petroleum Systems, Gravity Inversion, Potential Field Data, Gravity, Seismic, Magnetotellurics, SRTM, 2D and 3D forward Modelling**

----------**********----------

Introduction

1.1 Background

Eastern Cordillera of Colombia is a fold and thrust belt that evolved as a result of the Cenozoic Andean deformation (Colletta et al., 1990; Cooper et al, 1995; Mora et al., 2010). It is the eastern branch of the three Cordilleras the other two being the Central and Western (Sarmiento-Rojas et al., 2006; Mora et al., 2010). It consists of five structural domains namely; the Central Depressional Domain, the Western and Eastern Inverted Domains (anticlinoria) and the Eastern and Western Foothills (Sarmiento, 2011). To further understand the complex geologic structure of the area, Austin-Bridgeporth, a UK-based company which specialises in land, airborne and marine geophysical data acquisition, processing and interpretation, completed a series of magnetotelluric (MT) sections in late 2018 to early 2019. The magnetotelluric cross sections will complement the existing gravity and seismic data for frontier exploration purposes. This study therefore applies integrated geophysical approach to interpret the complex subsurface structural framework of the area and come up with a future prospectivity map for hydrocarbon exploration in the Eastern Cordillera.

1.2 Aim and objectives

1.2.1 Aim

The aim is to integrate the magnetotelluric data with the existing 2D seismic sections and existing gravity data to produce a hydrocarbon prospectivity map, and to provide a “road map” for future exploration activity.

1.2.2 Objectives

1. Review, integrate and interpret available datasets which are gravity, seismic, magnetotelluric as well as geologic cross sections.

2. Produce a qualitative interpretation using the available data.

3. Produce a series of interpreted 2D sections, depth surfaces and isopach maps utilizing all available datasets focusing on the thrust structures.

4. Produce 3D depth surfaces across the full survey area constrained by the 2D seismic, magnetotelluric and gravity data.

5. Produce a prospectivity map for future exploration programs.

1.3 Regional Geologic Setting

The northern Andean region of Colombia consists of three mountain ranges with distinct geological characteristics and age of formation (Toro et al., 2004). These are the Western Cordillera (Cordillera Occidental), Central Cordillera and the Eastern Cordillera (Cordillera Oriental). Most of the Central region which includes the Eastern Cordillera rests on the Paleozoic metamorphic rocks and Mesozoic to Cenozoic plutons overlain by deformed unmetamorphosed Cretaceous marine sediments (Toro et al, 2004).

A new oceanic spreading center was formed following the breakup of the Farallon plate to form the Nazca and the Cocos plates during the Late Oligocene to Early Miocene leading to increased rate of convergence in the Middle and South American trenches (Wortel, 1984; Lonsdale, 2005). According to Gregory-Wodzicki (2000), the Panama arc began to collide with the Northern Andes during the Middle MIocene resulting in an uplift of the Eastern Cordillera (see appendix A). Egbue and Kellogg (2012) reported that the Panama arc collision is probably the cause of the Andean orogeny in the Eastern Cordillera considering the timing, magnitude and direction of shortening. The collision was the beginning of inversion of the Mesozoic extensional structures, east- verging compressional structures in the Llanos foothills and the uplift of the Eastern Cordillera (Cooper et al., 1995, Taboada et al., 2000, Sarmiento, 2001, Mora et al., 2010).
Uplift and deformation are still going on in the Eastern Cordillera resulting in earthquakes in the foothills (Egbue and Kollogg, 2012). Coarse grained continental clastics of the Guayabo formation in the Llanos basin is an indication of recent erosion of the Eastern Cordillera (Cooper et al., 1995). Panama is colliding with South America at an average rate of 25 mm/year according to GPS studies (Trenkamp et al., 2002). However, present-day shortening in the Eastern Cordillera appears to have slowed to at most 12 - 4 mm/a and on the east flank of the Cordillera to only 4 - 2 mm/a (Trenkamp et al., 2002).

1.4 Location of Eastern Cordillera

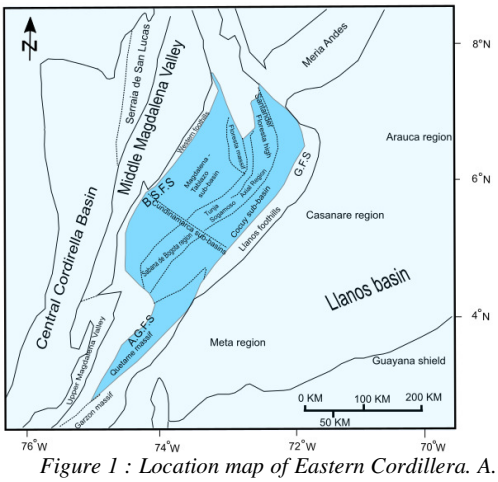

Figure 1 : Location map of Eastern Cordillera. A.G.F.S = Algeciras-Garzon fault System B.S.F.S = Bituima and La Salina Fault Systems, G.F.S = Guaicaramo Fault System(modified from Sarmiento, 2011).

Eastern Cordillera (ECB) is a northeast - southwest trending thrust belt that is 110 km – 200 km wide and it is bounded to the west and east by the Llanos and the Middle Magdalena foreland basins (Teixell et al., 2015). It is an asymmetric mountain range with a wider eastern flank and a 2.6 km wide of axial region dominated by high plateau with Sierra Nevada de Cocuy forming its highest elevation of about 4 km above sea level (Sarmiento, 2011). Its western limit is bounded by the Bituima and la Salina fault System (BSFS) while the east is limited by the Guaicaramo and Yopal faults. Strike slip faults of the Algeciras-Garzon Fault System (figure 2) forms its south-eastern boundary from the Llanos basin. Outcrops of Paleozoic basement rocks are seen on its northern and southern ends which corresponds to the Santander and Floresta massifs and the Quetame and Garzon Massifs (Sarmiento, 2011).

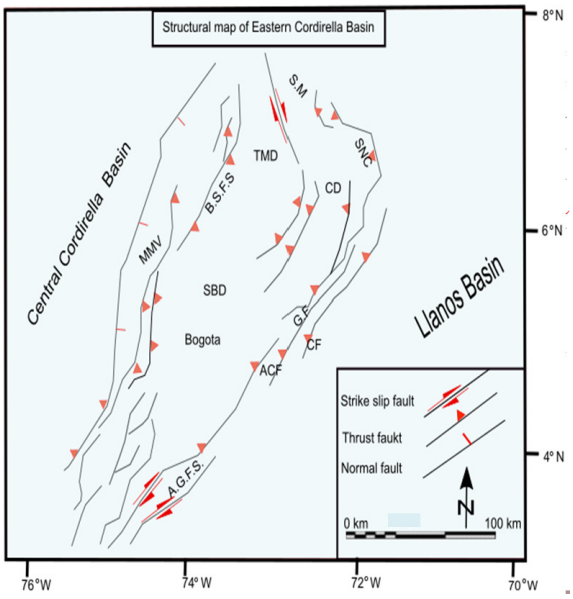

Figure 2: Fault distribution in the Eastern Cordillera. MMV = Middle Magdalena Valley, SNC = Sierra Nevada del Cocuy, TMD = Tablazo-Magdalena Depocenter, SBD = Sabana de Bogota Depocenter, SM = Santander Massif, CD = Cocuy Depocenter, ACF = Agua Clara Fault, GF = Guaicaramo fault, YF = Yopal Fault, Clara Fault, B.S.F.S = Bituima and la Salina Fault System, A.G.F.S. = Algeciras Garzon Fault System (modified from Cooper et al., 1995 and Barrero et al., 2007)

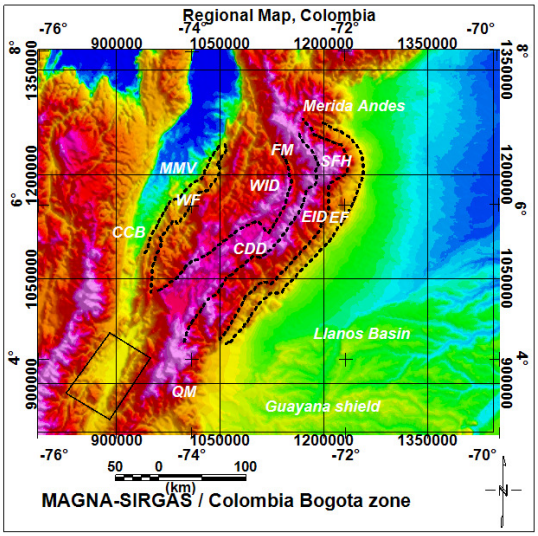

Figure 3: Structural domains of Eastern Cordillera overlain on Shuttle Radar Topographic Mission (SRTM) map. WF = Western Foothills, WID = Western Inverted Domain, EID = Eastern Inverted Domain, CDD = Central Depressional Domain, QM= Quetame Massif, SHF = Santander Floresta High, FM = Floresta Massif, MMV = Middle Magdalena Valley, CCB = Central Cordillera Basin. Structural domains modified from Repsol et al., 2002 (cited in Sarmiento, 2011). Rectangle on the South west corner shows the location of local survey domain gravity aero gravity data.

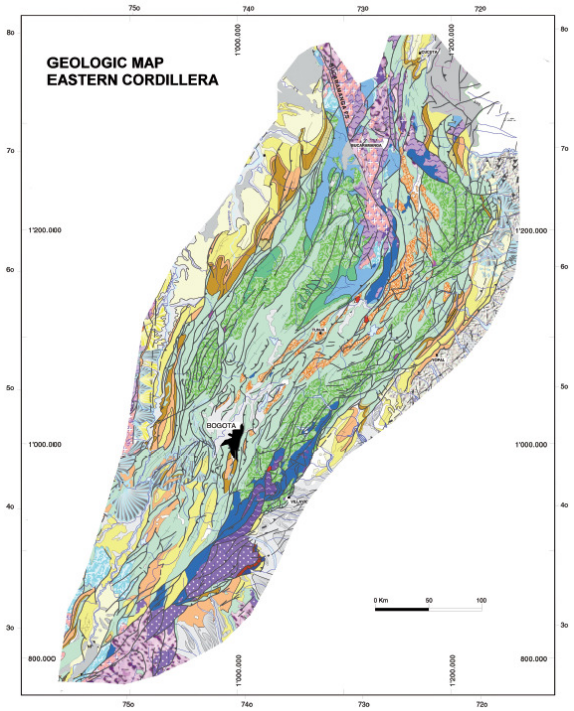

Figure 4: Geological map of Eastern Cordillera(after Geotec, 2000 cited in Sarmiento, 2011).

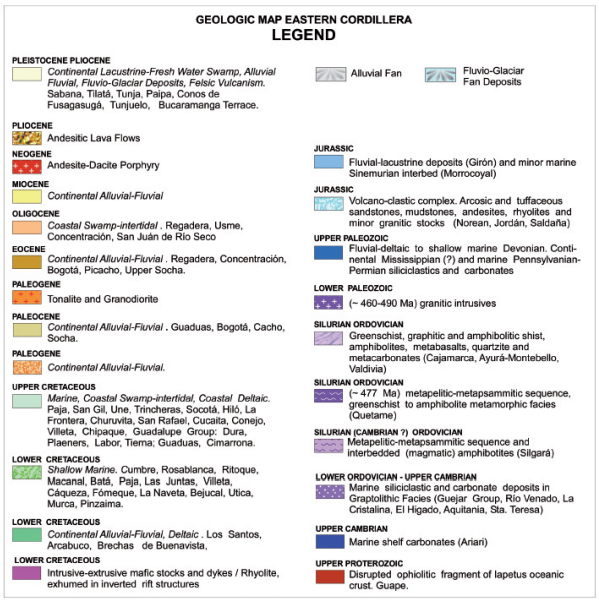

Figure 5: Legend of geologic map (after Geotec 2000 cited in Sarmiento, 2011)

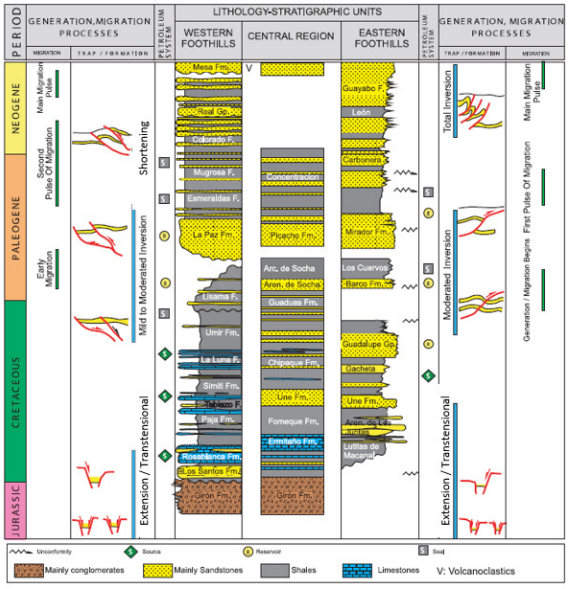

1.5 Tectonostratigraphy

Figure 6: Tectonostratigraphic chart of Eastern Cordillera modified from after Barrero et al., 2007.

1.5.1 Pre – Rift

The pre-rift consists of the lower crystalline basement (Paleozoic and Pre-Cambrian) and the economic basement (Upper Paleozoic to Jurassic) which comprises of meta-sediments (Sarmiento, 2011).

1.5.2 Mesozoic Extension

The exact onset of rifting is not well established since syn-rift clastic sediments are difficult to date and basin geometry is still uncertain (Egbue and Kellogg, 2012). Changes in lateral thickness of Mesozoic rocks suggest that the thrust faults that now define the eastern and western boundaries of the Eastern Cordillera were normal extensional faults (Sarmiento – Rojas et al., 2006; Mora et al., 2006, 2009). Isolated red beds, volcanic and volcano-clastics are seen throughout the basin and are believed to have been deposited in an elongated rift basin (Toro et al, 2004). The faults that bounded these rift basins can hardly be noticed as the compressional deformation of the Andes during the Cenozoic led to the inversion of the faults (Colleta et al., 1990; Cooper et al., 1995). Sarmiento-Rojas (2001) and Sarmiento-Rojas *et al.* (2006) back-stripped a total of 162 columns and wells across the Llanos, Middle Magdalena and the Eastern Cordilleras. The results of their analysis indicated the basins were stretched by five pulses that led to their evolution. Stretching values suggest that extensional stresses which may be related to the break – up of Pangea that eventually led to the separation of North and South Americas led to lithospheric stretching that created a narrow failed rift of less than 150 km that can be considered as an aulacogen basin (Cediel et al., 2003). New episodes of stretching in the Early Cretaceous trans-tensional stresses may have generated a wide probably greater than 180 km system of asymmetric half-grabens basins (Barrero et al., 2007).

1.5.3 Lower Cretaceous Rapid Subsidence

The rifting stage was followed by rapid subsidence and extension during the Neocomian (Lower Cretaceous) which led to accumulation of marine deposits within the Bogota basin most of which is occupied by the Magdalena Valley and the Eastern Cordillera (Fabre, 1987 cited in Teson et al., 2013). Separated by the Floresta – Santander massif, the northern Bogota basin was divided into two rapidly subsiding sub basins (Fabre, 1987 cited in Teson et al., 2013). The Cocuy sub-basin appears to be a half graben as Early Cretaceous subsidence rates were faster along the Guaicaramo fault system than the opposite end towards the Floresta massif (Sarmiento, 2002). Using the McKenzie model (1978), Fabre (1987) as cited in Teson (2013), proposed a stretching factor (beta) of two might have led to the rapid subsidence of the Cocuy basin. Detailed subsidence analysis of over 100 wells and surface sections indicates beta factor ranging from 1.1 to 3.0 with maximum stretching concentrated in an elongate trough parallel to the paleo Guaicaramo Fault System (Sarmiento, 2002). Elongated period of heat flow is indicated by numerous basaltic intrusions and high thermal maturation of the Early Cretaceous deposits (Fabre and Delaloye, 1982 cited in Toro et al., 2004).

1.5.4 Late Cretaceous to Paleocene Subsidence

As the lithosphere returns to thermal equilibrium, the Bogota basin continued to subside throughout the Cretaceous (Toro et al, 2004, Pindell and Tabbutt, 1995; Ojeda, 1996). Subsidence during

the Late Cretaceous is attributed to lithospheric cooling, water loading and horizontal compressional stresses that originates from the collision of oceanic terrenes in western Colombia (Sarmiento et al., 2006). Progradation of sandy deltaic and coastal facies (potential reservoirs) of the Albian Caballos, Une and equivalents started the transgressive – regressive megacycle (Toro et al, 2004). The peak of sedimentation was reached during the Turonian as the basement high separating the Cocuy sub-basin and the Tablazo were sub-merged with sediments extending to the east and western ends to feed the Llanos and Central Cordillera respectively (Villami, 1999). The same period witnessed the deposition of the regional northern South American anoxic marine shale source rocks which include the Cenomanian to Santonian Villeta, Gacheta, Chipaque and La Luna formations (Toro et al., 2004). A relative fall in sea level between Campanian and Maastrichtian led to the close of this megacycle followed by deposition of the Guadalupe sandstone group (Villamil, 1999). This sandstone group is productive reservoir both in the Llanos and the Upper Magdalena Valley. The thermal subsidence came to an end with the deposition of the Maastrichtian to Danian coal bearing deltaic to continental Guaduas Formation (Toro et al., 2004).

1.5.5 Cenozoic Basin Inversion

Thick oceanic crust of the Caribbean plate having separated from the Farallon plate began to move eastward relative to south American plate during the Late Cretaceous to Early Cenozoic (Burke et al., 1984). Eventually, it became subducted beneath the northern margin of Colombia (Pennington, 1981; Taboada et al., 2000). Compression and transpressive forces resulting from the interactions of the Caribbean–South American–Farallon triple junction led to the tectonic uplift of the Central Cordillera and inversion of the Bogota basin (Toro et al., 2004). Increased shortening since the Paleogene led to reactivation and inversion of the Mesozoic extensional faults which intensified in the Neogene leading to the evolution of the Eastern Cordillera mountain range (Colletta et al., 1990; Dengo and Covey, 1993; Cooper et al., 1995; Mora et al., 2006). Continental sedimentation began in the Eastern Cordillera during the Paleocene.

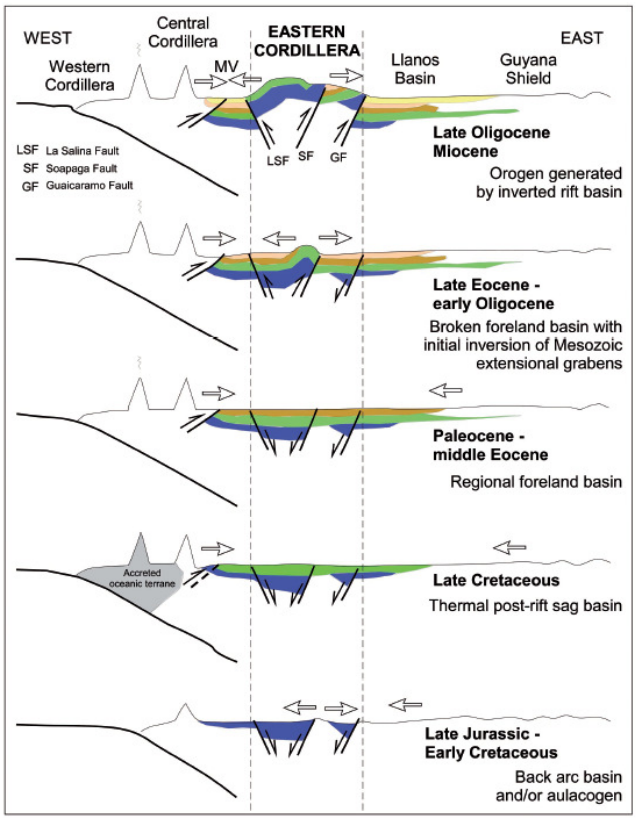

Figure 7: Tectonic evolution of the Eastern Cordillera (after Horton et al, 2010, cited in Sarmiento, 2011).

1.6 Petroleum System

1.6.1 Source Rocks

Main source rocks are the Aptian to Albian fine grained pelagic limestone and shale (Hilo Formation, Villeta Group, San Gil, Fomeque, Une Formation and lateral equivalents in the Eastern Cordillera) and the Cenomanian to Turonian deposits (La Luna, Churuvita, La Frontera, San Rafael, Chipaque formations and lateral equivalent in the Eastern Cordillera) which have T.O.C values ranging from 1.0 to 3.0% with a type I/II kerogen (Barrero et al., 2007). Global sea level rise in the Late Cretaceous coupled with anoxic upwelling favored the deposition of mudstones, cherts and phosphates of the Gacheta Formation, a prolific source rock that was deposited same time as the La Luna Formation (Haq et al., 1987; Villamil and Kauffman, 1993; Pindell and Tabbutt, 1995).

1.6.2 Reservoir Rocks

The sandstone of the Une Formation which represent one of the important reservoir rocks was deposited from Early Cretaceous to Cenomanian in a shallow marine environment (Cooper et al., 1995; Linares et al., 2009). Santonian to Maastrichtian Guadalupe

Group and lateral equivalents of the Eastern Cordillera and Paleogene sandstones of the Arenisca de Socha, Picacho and Guaduas formations (equivalents most productive in the Llanos and Middle Magdalena) are also important reservoir rocks (Sarmiento, 2011). The Guadalupe group is mainly progradational shallow marine shelfal sandstone unit that was deposited as a result of drop in global sea level (Linares et al., 2009). Average porosities and permeabilities of 5-10% and 4-100 md respectively were reported by Barrero et al., (2007).

1.6.3 Seal

Fomeque, Chipaque, la Frontera, Conejo and Guaduas formations mudstones and shales have seal potentials to the Une, Basal Une, Arenisca de Chiquinquira formations and Guadalupe group reservoirs (Sarmiento, 2011). The Cenozoic reservoirs are sealed by interbedded shale of the Socha formations (Barrero et al., 2007).

1.6.4 Migration

Migration occurred in two pulses; first in the Late Cretaceous and secondly, during the Miocene to recent. The first pulse was lost due to absence of trap at that time therefore, most of the giant fields of the foothills were charged during the second pulse (Barrero et al., 2007)

1.6.5 Trap

Fault propagation folds, thick skinned reverse faults and duplex structures form the main traps in the basin. (Barrero et al., 2007).

1.7 Prospectivity

The Cenozoic Andean deformation was probably related to strike slip motions and future discoveries may be trapped in structures formed as a result of transpression (Barrero et al., 2007). Main structural traps include fault bend fault, fault propagation fault and triangle zones as well as salt domes in the axial zone (Barrero et al., 2007).

1.8 Exploration History

The first exploration well in the Eastern Cordillera was drilled in 1948 to a total depth of 2128 m down to the Upper Cretaceous but was abandoned as dry and since then, a total of 36 wells have been drilled up till 2011 (Sarmiento, 2011). Only two wells drilled in 2007 and 2011 have been declared producers giving a success rate of 20% for that period according to ANH, 2011 (cited in Sarmiento, 2011). Most of the wells were dry with few having some oil shows.

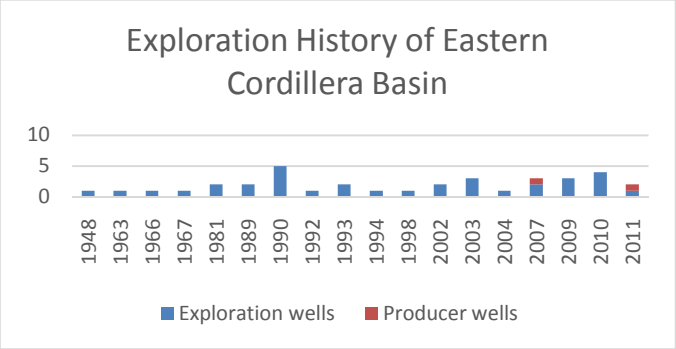

Figure 8: Exploration history of Eastern Cordillera Modified from Sarmiento (2011).

2. Database and Techniques.

2.1 Gravity Data

Principles of gravity data, free air and bouguer gravity anomalies are discussed in appendix B.

2.1.1 Gravity Effects of Simple Mass

Calculations of simple geometrical models helps in estimating the magnitude and type of gravity anomalies that geologic structures will display. Five simple geometric models including a horizontal cylinder, horizontal slab, rectangular prism, sphere and vertical cylinder are often used to predict wide range of geologic structures even though the actual shapes of structures rarely show a very close resemblance to the simple geometric forms (Sharma, 1986).

S/N	Simple geometric models	Predicted structures
1	Horizontal cylinder	Steep anticlines and buried ridges
2	Horizontal slab	Fault or step-like structure
3	Rectangular prism	Tabular bodies such as dikes
4	Sphere	Salt domes, compact and roughly equal dimensional bodies
5	Vertical cylinder	Salt domes and volcanic plugs.

Table 1:Gravity effects of simple mass (Sharma, 1986).

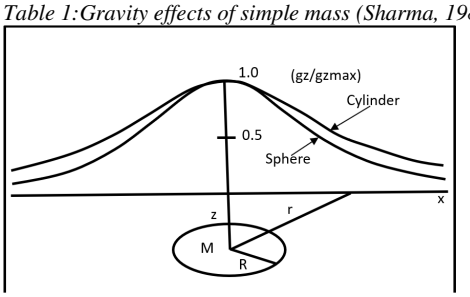

Figure 9: A model of gravity profiles of a sphere and a horizontal cylinder showing horizontal variation in gravity due to contrast in density. The maximum anomaly occurs where x = 0 and falls to its half value at x = x ½. Anomaly of a sphere is that of a mass at its center which equals the product of the density and volume of the

sphere. This model is the simplest illustration of non-uniqueness of the gravity field.

$$g = \frac{GM}{r^2} = \frac{GM}{x^2 + z^2}$$

$$g_z = gsin\theta = g\frac{z}{(x^2+z^2)^{1/2}} = GM\frac{z}{(x^2+z^2)^{3/2}}$$

$$M = \frac{4}{3}\pi R^3 \Delta\rho \quad \text{Equation 1}$$

so,

$$g_z = G\frac{4}{3}\pi R^3 \Delta\rho \frac{z}{(x^2+z^2)^{3/2}} \quad \text{Equation 2}$$

2.1.2 Source of Gravity Data

The Public domain dataset used in this project was obtained from the International Gravimetric Bureau (Bureau Gravimetrique International - BGI). Two survey data sets used were obtained from digitization of magnetic and gravity survey acquired by Carson Aerogravity (2009) with existing land and other airborne datasets while the other survey was obtained from Bridgeport. (See appendix B for survey grids)

2.2 Magnetotelluric Data

2.2.1 Principles

Magnetotelluric is an electromagnetic method which unlike the common induction method that have limited depth of penetration of few hundreds of meters, can map depths of hundreds of kilometers without requiring vast electrode arrays spread over long distances (Sharma, 1986). Magnetotelluric depth sounding is based on the natural currents also called telluric currents induced by the earth through fluctuating ionospheric currents in the earth. The flow of this current depends on the resistivity of the rocks it passes through. Resistivity values are obtained by measuring the electric field (E_x) on the ground surface in one horizontal direction and of magnetic field (B_y) in a horizontal direction at right angle to the electric field. Assuming the ground is uniform, the theory holds that:

$$\rho = \frac{0.2}{f}\left(\frac{E_x}{B_y}\right)^2 \quad \text{Equation 9}$$

Where ρ is in Ω, f is in Hz, E_x in mV/Km and B_y in nT (=γ)

2.2.3 Electrical Resistivities of Geologic Materials

Electrical resistivity tends to be the most varying property of rocks with magnitude in orders of 10s of ohms. Rocks composed of mostly silicate minerals tend to have high resistivity due to low electrical conductivities. Resistivity also largely depends on the porosity, permeability, moisture content, temperature, phase of pore fluid and dissolved electrolytes. Conductivities and electrical resistivities of some common rocks as shown in figure 10 will be used as a guide in interpreting the magnetotelluric cross sections in chapter six. Magnetotelluric method is mainly employed in the oil industry to estimate the thickness and electrical conductivities of sedimentary basins.

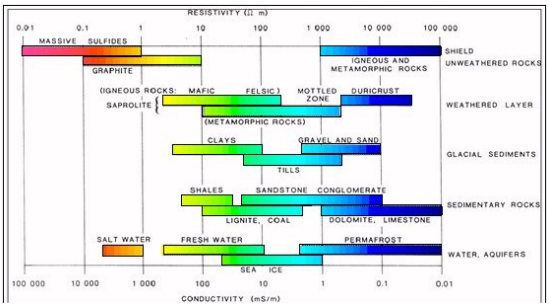

Figure 10: Electrical resistivity and conductivities of common rocks (after Palacky, 1987).

2.2.4 Source of Magnetotelluric Data

Three magnetotelluric lines used in this project were acquired by Bridgeport from 2018 to 2019 for an ongoing exploration campaign in the basin. Due to confidentiality of the datasets, the location maps for the cross sections cannot be published in this paper.

2.3 Seismic and Geologic Cross Sections

Most of the seismic sections are in the time domain and have been depth converted and reinterpreted where necessary for quantitative modeling. Geologic cross sections used were the product of field work and seismic interpretation. Due to confidentiality of the datasets, the location maps for the cross sections cannot be published in this paper.

3. Methodology

3.1. Qualitative Interpretation

Qualitative interpretation was aimed at identifying anomalous fields in the study area using the public and survey domains gravity data. Faults, lineaments, basement highs and lows were identified. Deep regional features as well as shallow structures were interpreted by applying filters at different wavelengths to the gravity data. The results obtained from the qualitative interpretation were used in 2D and 3D forward modeling for quantitative analysis.

3.1.1. Data Transforms

In order to separate the gravitational responses of targeted structures from the regional response, the data has been subjected to regional and residual gravity anomaly separation. Spatial and frequency filters were applied to obtain the transformations.

3.1.2. Bouguer Correction

This is carried out to adjust the measurement of gravitational acceleration to account for the effects of elevation and densities of rocks between a reference point and the measurement station. The grid obtained after the Bouguer correction is called the Bouguer anomaly grid. The gravity response from this map is reflective of the densities of rocks in the subsurface. Density correction of 2.67 g/cc was used as a global average for public domain data while correction of 2.55 g/cc was applied to the digitized aero gravity data.

3.2. Quantitative Interpretation

3.2.1. 2D Forward Modeling

2D forward modeling was carried out on twenty seismic lines, five geologic cross sections and three magnetotelluric lines. It was aimed at integrating these lines with the field gravity data in order to define the thickness of sediment cover. It also helps in identifying the source of anomalies earlier identified in the qualitative interpretation and allows for modifications to be made on to the qualitative interpretation where necessary. A geologic model is created using the information from the modeled lines to establish a best fit between the calculated and observed gravity responses. Several simple model scenarios were created as first attempts to see the possibilities of finding the simplest and geologically realistic models.

3.2.2. Horizon Mapping

Depth surfaces of Top basement, Top Cretaceous and Top Tertiary were calculated using the 2D models constrained with the observed gravity response and SRTM data at an extrapolation of 10,000 m.

3.2.3. 3D forward Modeling

A 3D model was built from the horizons obtained from 2D modeling using the digitized gravity data as an observation model. Depth surfaces of the Top Basement and Top Cretaceous generated from the inversion model identified the trends of the main thrust and areas of thick sediment covers. The 3D surface is generated with the assumption that the input signal emanates from a single interface. In order to avoid anomalies, multiple corrections are carried out before the depth maps were finally generated. The corrections accounted for include the gravity effects of long regional wavelength signals that originate from the Moho and short wavelength anomalies attributed to shallow structures. Sediment thickness maps were obtained from the inversion model.

3.2.4. Moho and SRTM Data

The Moho data was obtained from a public domain source (Crust 1.0). It helps in identifying the depth to top Moho across the study area and allows for estimation of crustal thickness. Correction for the effects of long regional wavelength signals from the free- air gravity data was also made using the Moho data. The Shuttle Radar Topographic Mission (SRTM) data also sourced from public domain is used to map surface topography across the study area.

4.0 Regional Qualitative Gravity Data Interpretation

Regional qualitative interpretation was conducted on the public domain data from BGI and the digitized survey domain data from Graterol and Carson (2009).

4.1 Public Domain Gravity Interpretation

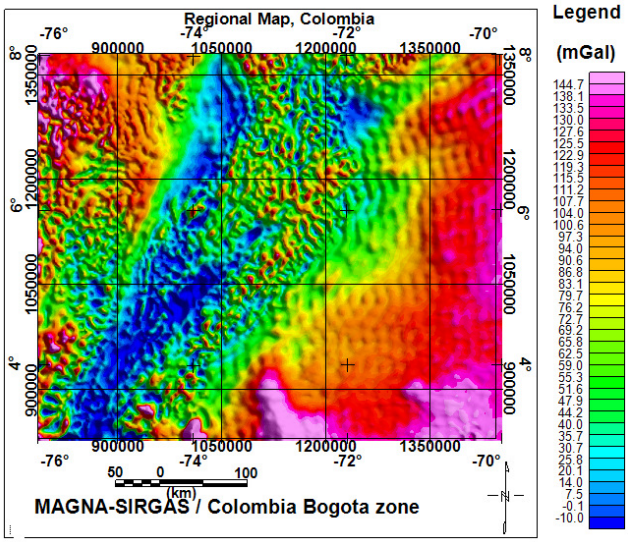

Figure 11: Regional bouguer gravity anomaly map of Eastern Cordillera (Source International Gravimetric Bureau).

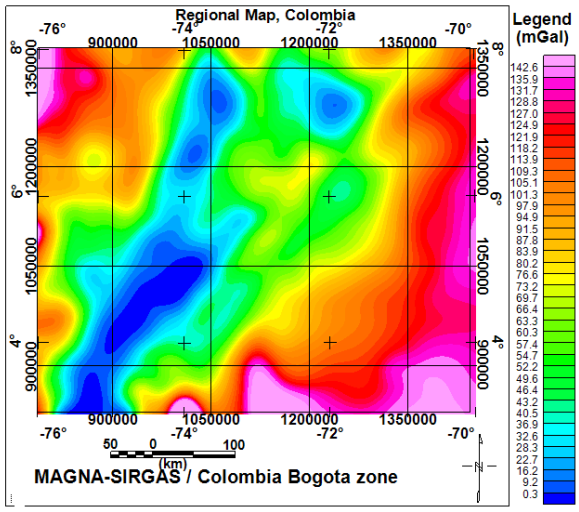

Figure 12: Bouguer gravity anomaly map at 100 km low pass filter

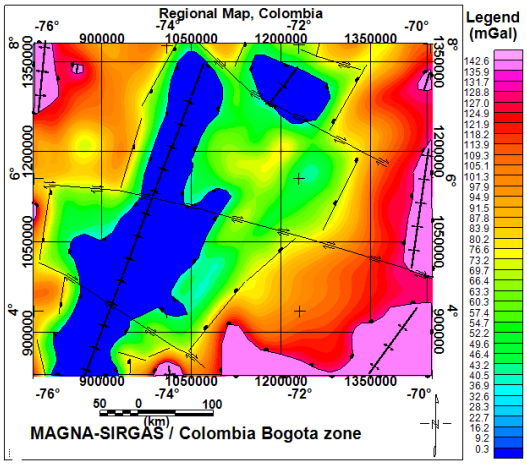

Figure 13: Bouguer gravity at 100 km low-pass filter showing regional structural settings

The bouguer gravity at 100 km low-pass filter shows deep-seated regional features which roughly correspond to the gravity response of the Moho. Extreme gravity lows and highs are highlighted with blue and pink polygons respectively. A NE-SW trend can be seen in the general orientation of the basin. Using simple edge detection technique, NE-SW trending fault and lineaments roughly perpendicular to the fault direction were mapped.

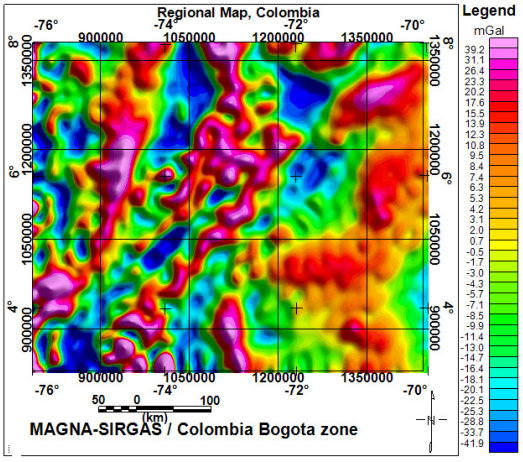

Figure 14: Public domain bouguer gravity anomaly map (filter wavelength = >30 km and <300 km)

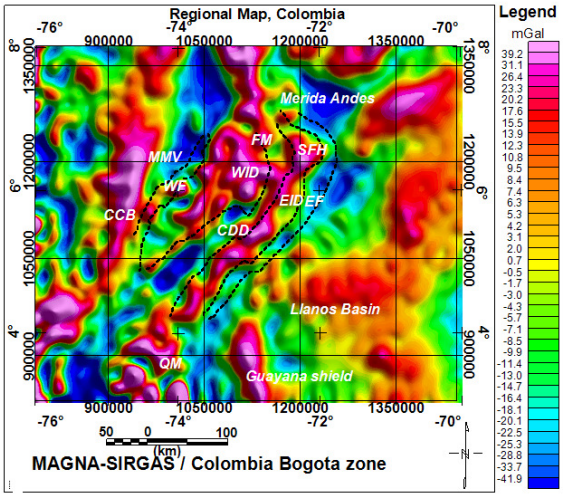

Figure 15: Public domain Bouguer gravity anomaly map (filter wavelength = >30 km but <300 km) overlain with structural domains. WF = Western Foothills, WID = Western Inverted Domain, EID = Eastern Inverted Domain, CDD = Central Depressional Domain, QM = Quetame Massif, SHF = Santander Floresta High, FM = Floresta Massif, MMV = Middle Magdalena Valley, CCB = Central Cordillera Basin.

At a filter range >30 km and <300 km, the depocenters in the Sabana de Bogota and Merida Andes appear prominent. The Quetame and the Floresta highs both stand out as gravity highs. The Middle Magdalena Valley in the north-west and the Central Cordillera Basin also correspond to lows and highs respectively. the Western and Eastern Foothills predominantly correspond to gravity lows.

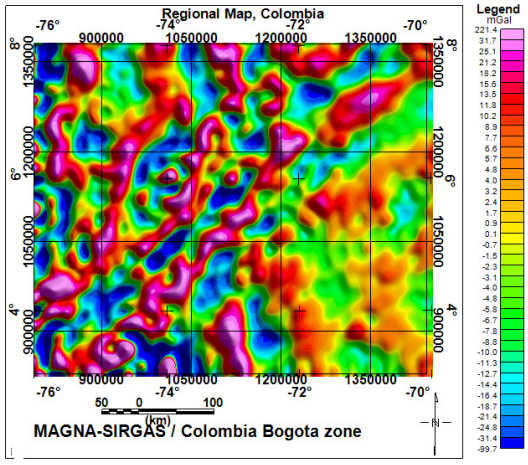

Figure 16: Public domain Bouguer gravity anomaly map (filter wavelength = >30 km but <150 km)

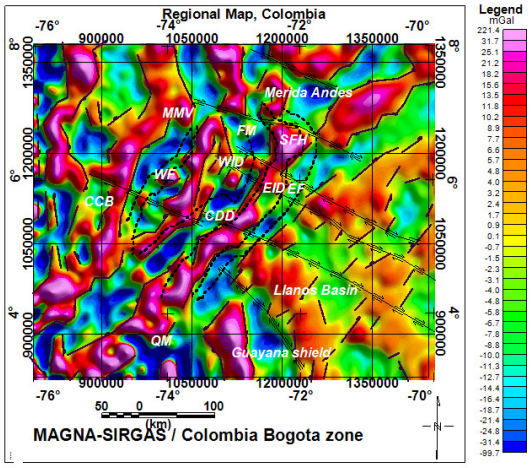

Figure 17: Public domain Bouguer gravity anomaly map (filter wavelength = >30 km but <150 km) with structural interpretation. WF = Western Foothills, WID = Western Inverted Domain, EID = Eastern Inverted Domain, CDD = Central Depressional Domain, QM= Quetame Massif, SHF = Santander Floresta High, FM = Floresta Massif, MMV = Middle Magdalena Valley, CCB = Central Cordillera Basin

Application of a filter at a range >30 km but <150 km removed the effects of deeper gravity responses while enhancing the structural trends of shallower features as compared to figure 15. The dominant fault trend is NE-SW with E-W trending lineaments. The structural domains are more pronounced with lows in the CDD extending into the northern side which corresponds to the Sabana de Bogota depocenter (figure 1). The Eastern and Western Foothills domains also coincide with gravity lows. This result indicates that previous gravity highs observed in the foothills in figure 15 were simulated by deeper materials.

4.2 Digitized gravity Interpretation

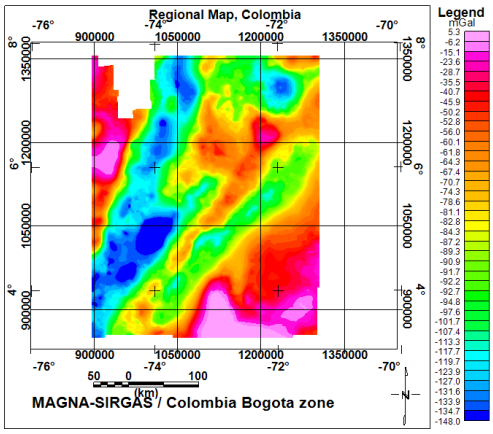

Figure 18: Digitized bouguer gravity anomaly map with a density correction of 2.55 g/cc obtained (Graterol and Carson Aerogravity, 2009)

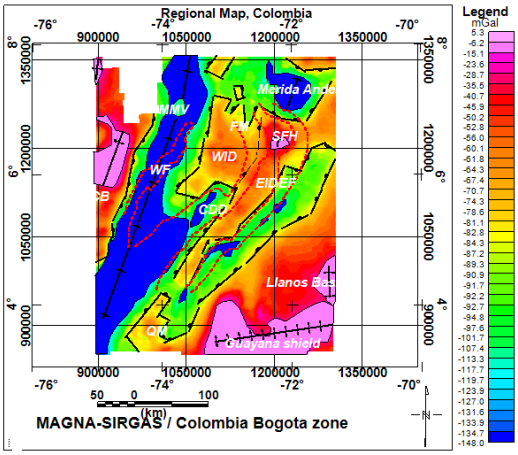

Figure 19: Structural interpretation of digitized bouguer gravity anomaly map. WF = Western Foothills, WID = Western Inverted Domain, EID = Eastern Inverted Domain, CDD = Central Depressional Domain, QM= Quetame Massif, SHF = Santander Floresta High, FM = Floresta Massif, MMV = Middle Magdalena Valley, CCB = Central Cordillera Basin

Extreme gravity lows can be seen as hightlighted with blue polygons (Figure 9). The gravity high in the north central part of the map corresponds to the Santander and the Floresta massifs while the highs towards the southwest corresponds to the Quetame massif. The largest gravity low on the western half covers the geographic locations of the Sabana de Bogota, Magdelena Tablazo sub-basin, Western Foothils and the Tunja Sogamaso basins and extends northwards into the Middle Magdalena Valley (see figure one for geographic locations). The lows at the NE corner of the map is in the domain of the Merida Andes. Gravity highs at the NW and SE correspond to geohgraphic locations of the Central Cordillera and the Llanos basin respectively. Guayana shield in the southern corner of the map exhibits the highest and largest gravity respond.

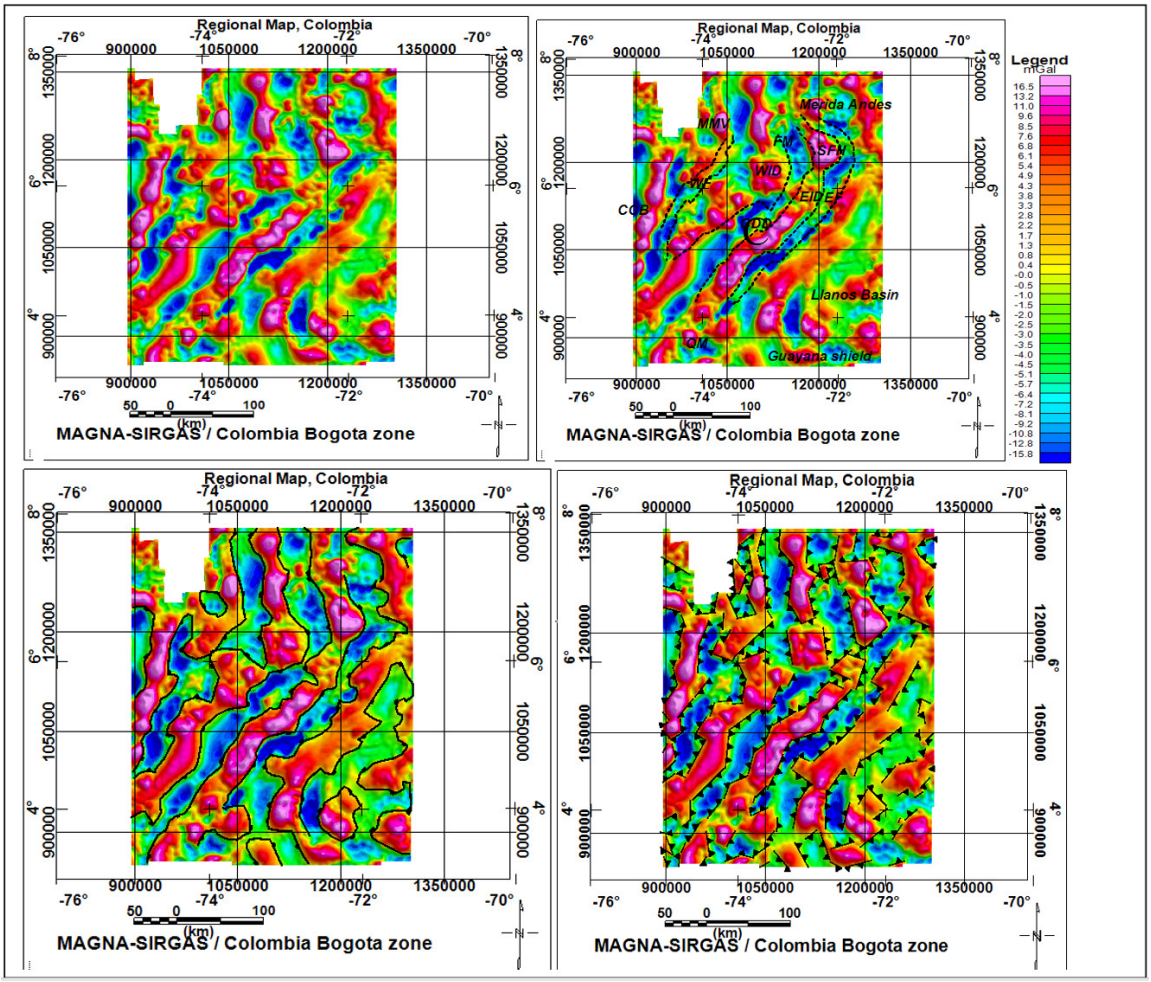

Figure 20: Digitized bouguer gravity anomaly map showing structural trends (filter range = >10 km but < 100 km). WF = Western Foothills, WID = Western Inverted Domain, EID = Eastern Inverted Domain, CDD = Central Depressional Domain, QM= Quetame Massif, SHF = Santander Floresta High, FM = Floresta Massif, MMV = Middle Magdalena Valley, CCB = Central Cordillera Basin

Many structural features at shallower depth began to manifest more prominently. The Quetame massif, the Santander Floresta Massif, the Guayana shield of eastern Llanos basin, Inverted Western and Eastern Domains of the Eastern Cordillera and the Central Cordillera Basin all stand out as gravity highs as shown in panel B. The Central Depressional Domain (CDD) now appears in a complete gravity low which indicates the earlier highs observed in the middle of the CDD were simulated by deeper materials. Panels C and D show regional structural NE-SW trend and some N-S trends in the northern part.

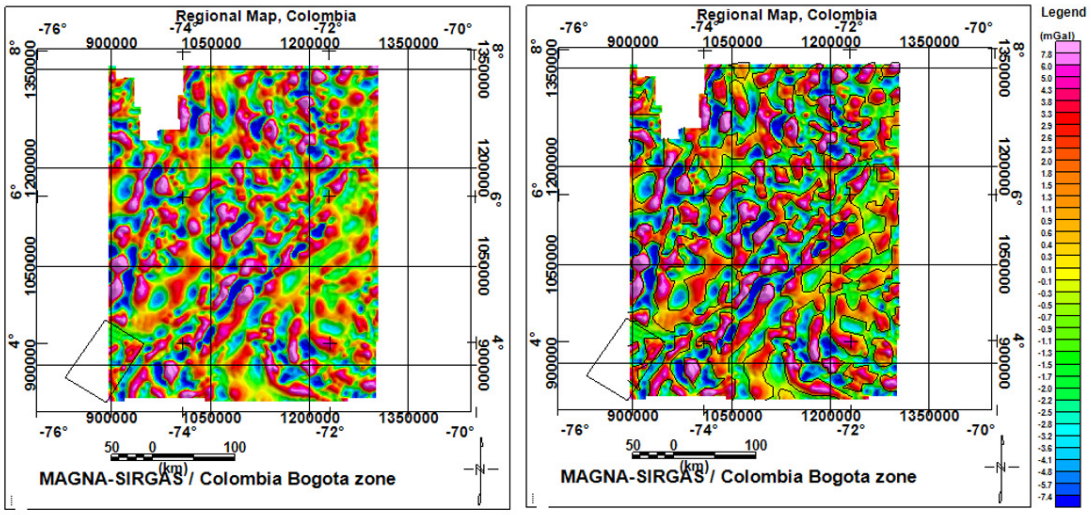

Figure 21: Digitized bouguer gravity anomaly map (filter range >10 km but <50 km)

Panels A and B show the shallowest qualitative interpretation carried out using the digitized map. Complex and isolated structures are seen within a short distance with patchy gravity highs and lows attributed to shallow seated materials.

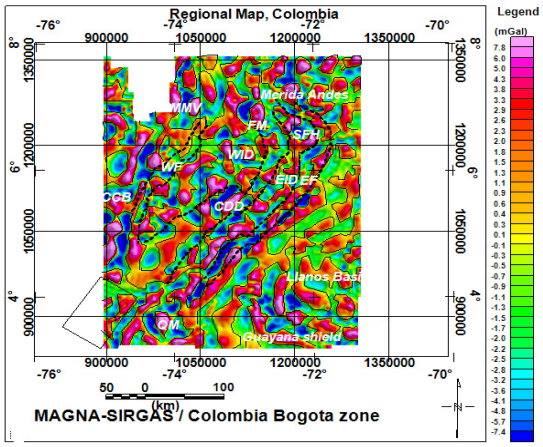

Figure 22: Digitized bouguer gravity anomaly map (filter range >10 km but <50 km) overlain with structural domains of Eastern Cordillera. WF = Western Foothills, WID = Western Inverted Domain, EID = Eastern Inverted Domain, CDD = Central Depressional Domain, QM= Quetame Massif, SHF = Santander Floresta High, FM = Floresta Massif, MMV = Middle Magdalena Valley, CCB = Central Cordillera Basin

It can be seen from figure 22 above the depressions on the center of the Santander Floresta High (SFH), the Guayana shield in Llanos basin and the Central Cordillera Basin. Conversely, the Quetame massif appears to be isolated in the middle of gravity lows. The inverted domains of the Eastern Cordillera also appear to be patchy.

4.3 Summary of Regional Gravity Data Interpretation

4.3.1 Structural Mapping

The Eastern Cordillera is divided into five structural domains which are the Western and Eastern Foothills, the Western and Eastern Inverted Domain and the Central Depressional Domain. Structural mapping of the area was conducted by edge detection between contrast in response of gravity lows and highs which correspond to basement lows and highs. Structural domain mapping from previous works were also overlain on the bouguer anomaly maps. A dominant NE-SW trending faults is observed throughout the basin. W-E trending lineaments were observed in the regional long wavelength anomaly maps. As the main tectonic regime of this basin is thrust, most of the faults were interpreted as thrust faults. More structural features appear with decrease in wavelength, this allows for mapping of structures that are shallow in origin and the structures increase in complexity as was observed with the evolution of the structural domains, the Quetame massif, the Santander Floresta high and the Eastern Llanos Guayana shield. Structures that tend to overlay on long and short wavelengths are simulated by deep seated regional features that have their tops close to the surface while those that appear only on the short wavelength anomaly maps are shallow in nature and vice versa.

4.3.2 Basin Mapping

Using the edge detection technique, gravity lows and highs were mapped throughout the two datasets to show structural trends of basins within the regional map. Areas with high gravity signals have high tendencies of being basement highs while corresponding lows are very possibly areas with thick sediment covers. This is a quick way to identify basins, their trends and shapes using gravity data.

4.4 Uncertainties of Regional Gravity Data

The public domain data was obtained at a low resolution and as such is less reliable. The digitized maps were obtained at high

resolution and have higher degree of reliability. The two datasets tend to agree with one another in the structural trend and distributions of gravity highs and lows which increases the confidence in the datasets.

5. Local Survey Gravity Data

5.1 Overview of the data

The survey was carried out over an area of roughly 100 km by 65

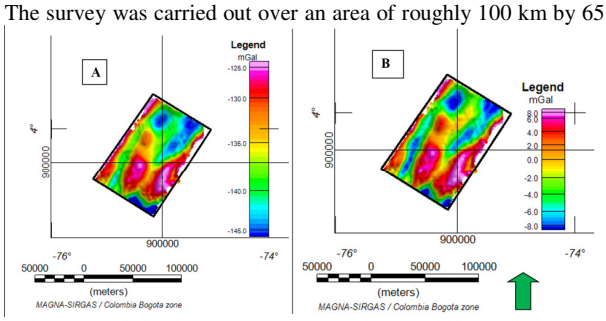

Figure 23: Survey domain free air gravity anomaly map A (unfiltered) and B (long wavelength filter at 100 km).

kmat a 1 km x 10 km line spacing at the south western part of the study area. The data has been subjected to regional and residual gravity anomaly separation. Spatial and frequency filters wereapplied to obtain the transformations. A density correction value of 2.67 g/cc was applied as global standard.

5.2 Comparison with regional gravity dataset

Although this survey data was carried out over a relatively small area, the main structural trend observed in the regional maps is retained on this data. The data shows that if extrapolated, it is very likely that it can maintain the same trend throughout the study area at a higher resolution. This increases the degree of confidence in the three datasets. Comparing high resolution survey domain data to that of relatively low-resolution data is a way of constraining uncertainties in gravity data interpretation.

5.3 Summary of local survey domain interpretation

Residual anomaly maps were generated using the same procedure followed for the regional data. Residual gravity maps of wavelengths 15 km, 25 km, 50 km and 100 km were created to allow for qualitative analysis at different wavelengths. Edge detection mapping was used to distinguished basins and basement highs which correspond to gravity lows and highs respectively. Dominant structural trend of NE-SW just as in the regional data is retained.

5.4 Uncertainties

This survey was carried out over a relatively small area at a line spacing of 1 km x 10 km. It was carried out at a high resolution and as such has higher degree of precision and therefore more

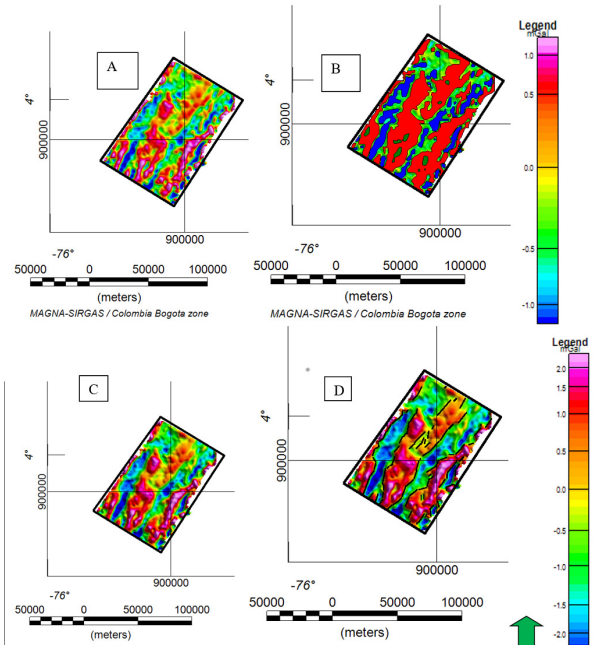

Figure 24: Bouguer gravity anomaly maps of survey domain data. (filter wavelength = >15 km but <25 km).

Panels A and C are anomaly maps at Gaussian filter of 25 km and 15 km with corresponding interpretation of highs and lows and structural trend mapping on panels B and D respectively. NE – SW dominant trend can be observed just as in the public domain data.

reliable when compared to the regional data with minor associated uncertainties.

5.5 Summary of qualitative interpretation

Qualitative interpretation allowed for a quick way of evaluating the distributions of geologic features across the study area. The structures obtained from the qualitative analysis agrees with the distributions of structures reported in literatures showing a dominant NW-SE trend. Evolution of the main features and the structural domains such as the Central Depressional Domain (CDD), Eastern and Western Foothills, the Eastern and Western Inverted Domains, the Bogota, Tablazo and Magdalena depressions have been seen through the application of filters at different wavelengths. The Quetame massif, the Santander massif and Floresta highs all stand out as gravity highs. The results obtained can now be used with seismic, magnetotelluric and geological cross sections to produce 2D and 3D forward models for quantitative analysis.

6.0 Quantitative Interpretation

6.1 2D Quantitative Interpretation

2D forward modeling was conducted on 20 seismic lines, 5 geological cross sections and 3 magnetotelluric lines. 2D modeling allows for integration of information using a seismic, geologic and/or magnetotelluric section alongside a gravity profile to come up with a calculated model that fits the observed

gravity response. It also integrates the depth of the top Moho imported from public domain source (Crust 1.0) and Shuttle Radar Topography Mission (SRTM) altitude map also from public domain. The modeling is done in a way that it allows for reinterpretation of the seismic, geologic or magnetotelluric section in a geologically realistic manner. The degree to which a reinterpretation will be needed differs from line to line. The modeling is not aimed at a perfect fit, rather a best fit that honors both the section as well as the gravity profile. The end models were used to generate depth surfaces and subsequently thickness maps.

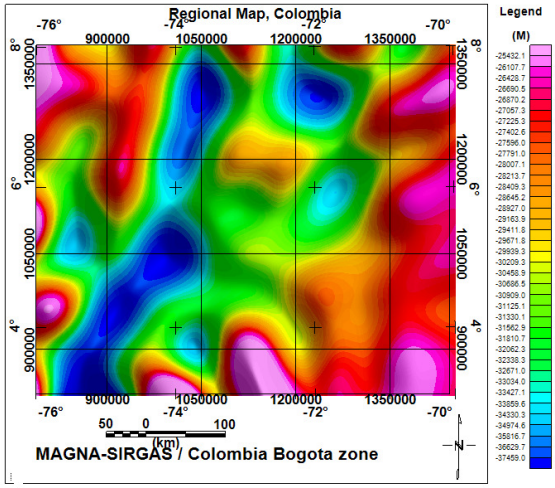

Figure 27: Depth horizon of Top Moho imported from Crust 1.0

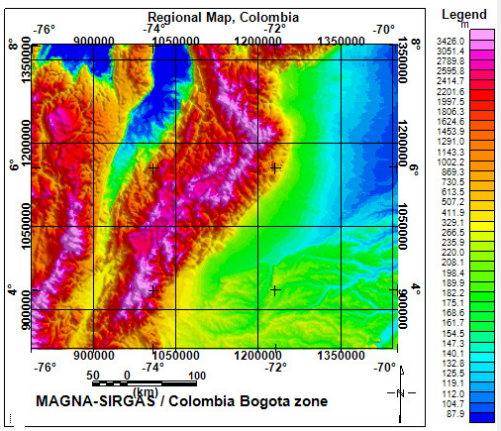

Figure 28: Regional Shuttle Radar Topography Mission (SRTM) used in quantitative analysis.

6.1.1 Depth Conversion and Velocity models

Of the 20 seismic lines, only two are in depth while the remaining 18 lines are in time. The time models must be converted to depth before a calculated gravity model can be obtained. A four-layer velocity model was used for the depth conversion.

S/N	Layers	Unit	Average Density (g/cc)	Seismic Velocity
1	First layer	Cenozoic	2.4	4,000 m/s
2	Second layer	Mesozoic	2.5	4,600 m/s
3	Third layer	Basement	2.7	5,700 m/s
4	Fourth layer	Moho	3.3	7,900 m/s

Table 2: Values used for velocity model: density values were obtained from literatures (Veiga and Dzelalija 2014; Kellogg et al., 2005) and density – velocity conversion was done using approximate conversion factors from Barton (1986).

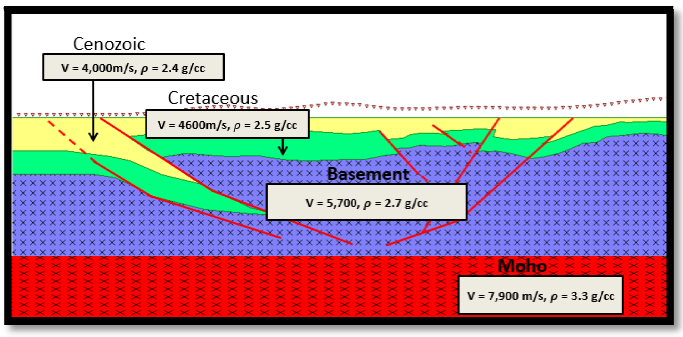

Figure 29: Four-layer velocity model used for depth conversion.

6.1.2 Test Model

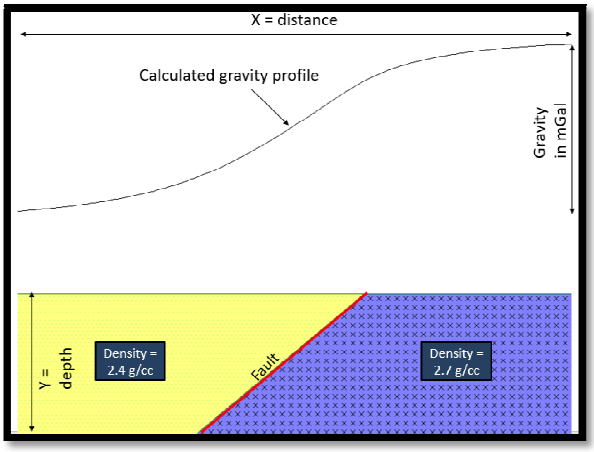

Figure 30: Test model

In order to ascertain that the model is working based on change in gravity with density, a simple slab model of a sediment layer juxtaposed against a basement rock was used. The model shows that the Oasis Montaj software is responding to change in density accordingly. This was followed by sensitivity test to know the main factor that affects the gravity response in the model. The density values obtained from analogue data were applied. The

first stage of the sensitivity test was to determine the response that is attributed to the Moho by applying a long wave length low pass anomaly filter. The Moho is then adjusted appropriately within a range of +/- 3km. The calculated and observed responses were then fitted even though the variation between the two are mostly minimal and in some cases negligible as they tend to fit even without any changes applied. Secondly, gravity values are varied for the basement rock and the sediment cover to see which one has the greatest effect in the gravity response. The test shows that the basement rocks having a density value of 2.7 g/cchas the greatest effect in the gravity response while the sediment having values ranging from 2.6 - 2.4 g/cc have lesser effect. The Moho tends to have the least effect due to its depth despite having a gravity value of 3.3 g/cc. The sensitivity tests applied are illustrated using line SFIG10N in figures 32, 33 and 34.

6.2 2D Modeling Procedure

Modeling was carried out on 20 seismic lines, 5 cross sections and 3 magnetotelluric lines. The first stage of model is to interpret the sections. Generally, three lithologic units were considered to obtain a simple model that will fit the observed gravity model. The units are basement complex (unit one), Mesozoic unit which is mostly composed of Cretaceous sequence (unit two), and the Cenozoic (unit three). This is followed by importation of the depth of top Moho from public domain source (Crust 1.0). Gravity values obtained from analogue sources were assigned to each unit (table four). A gravity calculation is run which then produces the result for both the observed gravity from the digitized data and the calculated gravity response from the model using the depth and the gravity values assigned. In most cases, the two responses will trend in the same manner. Reinterpretations of the sections were conducted in sections that tend to vary. Most of the reinterpretations take place on the top basement as the sensitivity test shows that the basement has the highest effect on the gravity response. The sedimentary layers were also reinterpreted where necessary.

6.2.1 Evolution of 2D Models

Different cross sections are presented and discussed in this section. Seismic section SFIG10N is used to illustrate the details of steps taken towards obtaining an end model for each section.Each model goes through several interpretations constrained with gravity data and the density values assigned. This allows for integration and produces an end model that honors all available datasets.

6.2.2 Seismic line SFIG10N

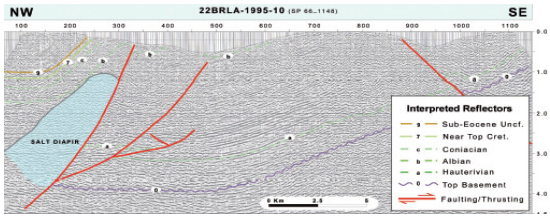

Figure 31: Seismic line SFIG10N (Ecopetrol et al., 1998).

This line was originally interpreted to have a salt diaper as shown in figure 31 above. It was interpreted to have shown the basement rock overlain by the Cretaceous while the Cenozoic tops the section. An initial model that honors the exact literature interpretation was developed. To calculate the gravity responses from the model, it was converted to a depth domain using velocity values in table four. The result obtained from the first model shows a fair match except for the area where the salt occurs as shown in figure 31. The model was reinterpreted to have no salt and the result shows a very good match and geologically realistic. The presence of salt from the seismic data itself is not convincing as salt tends to give a chaotic reflection due to its seismic velocity and exhibits strong contrast with surrounding lithologies which is difficult to establish in the seismic above. Moreover, the observed gravity response shows a flat line indicating no presence of low-density material of that size in the section. Salt has an approximate density of 2.1 g/ccwhich makes it significantly lower than the surrounding sediment which has density of 2.5 g/cc. A drop in gravity response similar to a simple geometry model such as a sphere or cylinder occurs where salt domes are present as described in table 1.

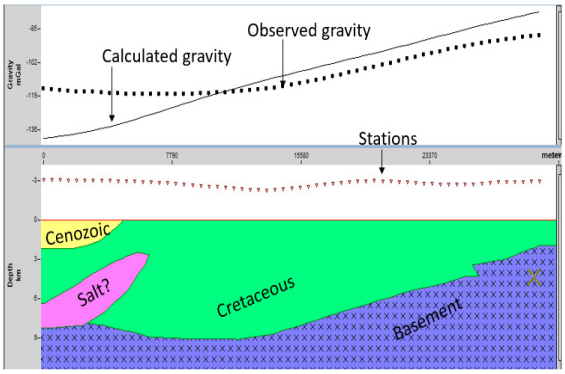

Figure 32: Initial model of seismic line SFIG10N

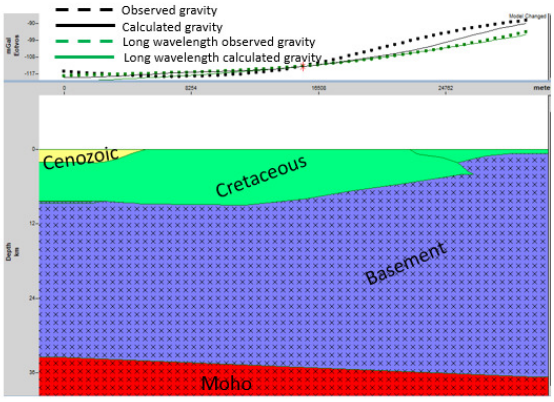

Figure 33: Second model of seismic line SFIG10N.

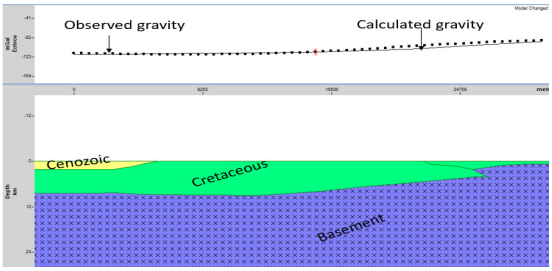

Figure 34: Second model of seismic line SFIG10N with adjusted Moho depth. After the long wavelength observed and calculated gravities where matched, the calculated and observed gravity responses exhibit a good match.

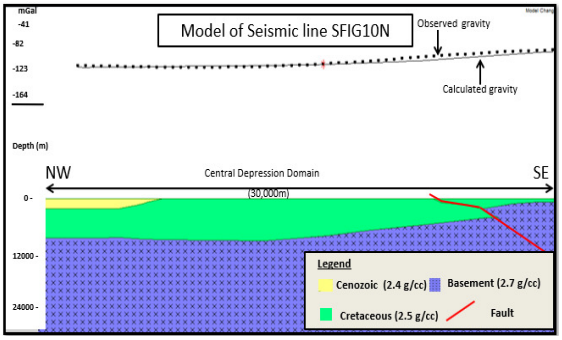

Figure 35: Final model of seismic line SFIG10N

A final model is obtained after all necessary modifications have been made. Line SFIG10N is a NW-SE trending line that is in the Central Depressional Domain of the Eastern Cordillera. The surface geology of the line is checked with the geologic map to further increase the confidence in the interpretation. The bouguer gravity anomaly map overlain with seismic layout is also used to double check the gravity response.

6.2.3 Seismic line SFIG2N

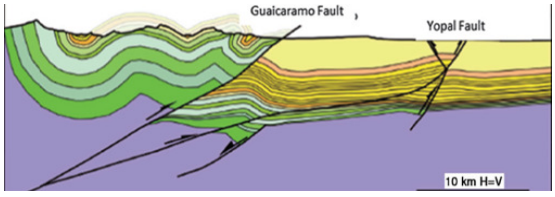

Figure 36: Seismic section of line SFIG2N (Garcia et al., 2015).

The above line is a depth seismic line that extends from the eastern inverted domain of the ECB to the eastern foothills (from left to right) with the Guaicaramo fault as a boundary between the two domains. The uninterpreted seismic line was not available which makes it difficult to make a well-informed adjustment.

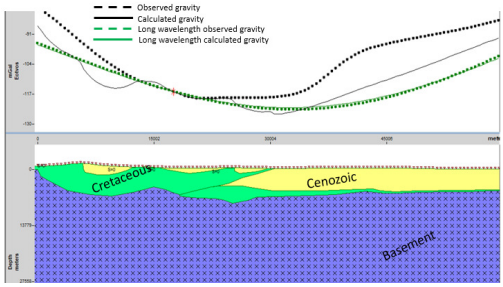

Figure 37: Initial model of seismic line SFIG2N

First model was interpreted to account for 3 lithologic units. The Moho was adjusted so that appropriate adjustment could be made to the basement and the sediment cover to come up with a best bit. As shown in figure above, there is a variation between observed and calculated gravity response. Sensitivity response indicated that the variation is largely due to the densities in the sediment cover and a second model was developed as shown in figure 38 below.

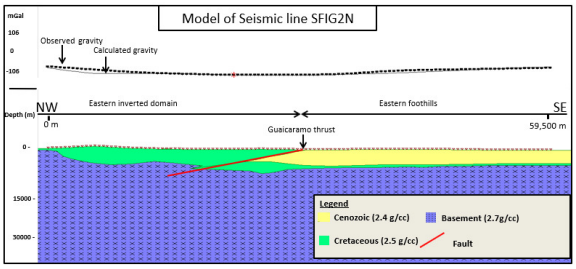

Figure 38: Final model of seismic line SFIG2N

The final model considered simplification of the sediment cover. The Cenozoic unit in the left-hand side of the first model which was given a density value of 2.4 g/cc was considered as part of the Cretaceous and was re-assigned a density value of 2.5 g/cc. The surface geology map overlain with the seismic layout showed no presence of the Tertiary unit over the Cretaceous along the seismic profile.

6.2.4 Magnetotelluric (MT) Line 2N

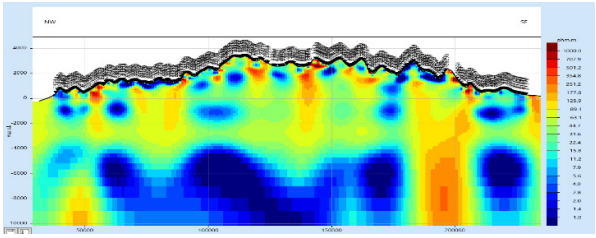

Figure 39: Cross section of MT Line 2N. See figure 25 for location.

The colors in the MT cross section above change with change in resistivity of the rock the telluric current is passing through. Generally, unweathered basement rocks such as igneous and metamorphic, sedimentary rocks such as dolomite, limestone and conglomerate exhibit high electrical resistivity (figure 10). Lithologies containing water, clays, shales, coal, coal, graphite and sandstones tend to have low electrical resistivity (figure 10).

The wide range of resistivity values across lithologies makes it difficult to identify specific lithologies, however, deep seated highly resistant units can be interpreted as basement rocks and shallow low resistant units as sediment cover. To further constrain uncertainty in the interpretation of the MT section, an adjacent seismic or geologic cross section is used.

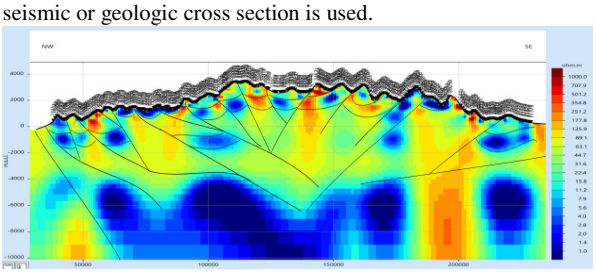

Figure 40: Interpreted Cross section of MT Line 2N

The figure above shows an interpreted section of MT Line 2. This interpretation is mainly based on the trends that can be observed from the section itself.

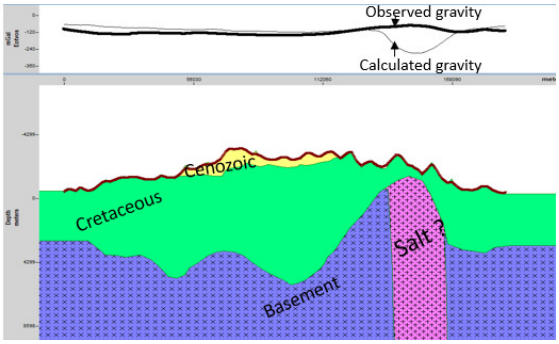

Figure 41: Initial model of MT Line 2N

The initial model considered the low resistivity response on the *eastern end of the line as a salt dome since salt is found in the stratigraphy of the basin. The calculated gravity response and the observed varied significantly which shows that the low resistivity respond is not as a result of low density and low resistance lithology such as salt.*

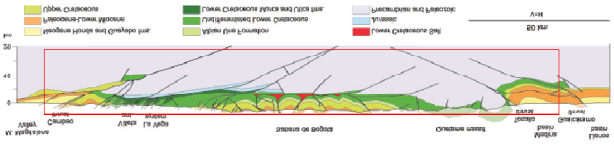

Figure 42: Geologic cross section of SFIG22N (Teixell et al., 2015).

The above geologic cross section runs south of MT line 2N trend NW – SE parallel to MT Line 2. The red rectangle shows the exact distance that corresponds to MT Line 2. The cross section together with the observed gravity model were used to constrain uncertainty in creating a model for MT Line 2.

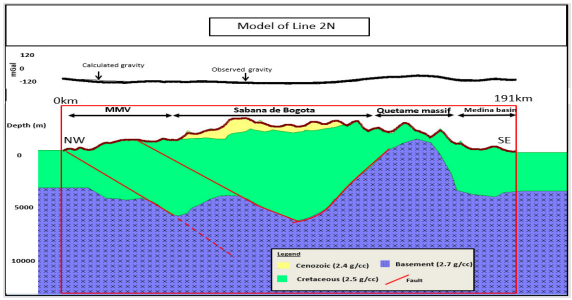

Figure 43: Final model of MT Line 2N.

The integration of the MT line, geologic cross section, surface geology map and observed gravity led to the generation of a best fit model that does not only honor the data set employed but also created a calculated model that is almost as exact as the observed gravity response. The low resistance zone earlier interpreted as salt dome in figure 41 has been reinterpreted to be a basement high which corresponds to the Quetame massif in the geologic cross section. The low resistivity signal given by the zone is probably due to it being weathered and containing water.

6.2.5 Cross section SFIG21N

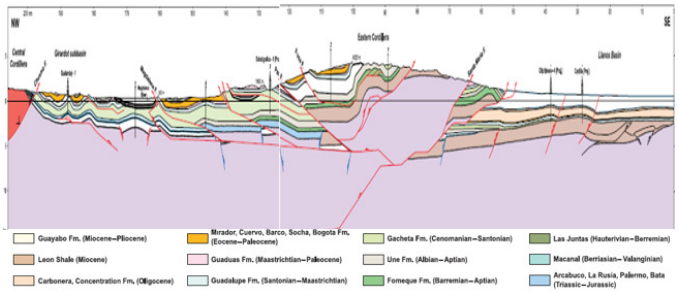

Figure 44: Geologic cross section SFIG21N (Toro et al., 2004). See figure for 25 for location.

Cross section SFIG21N is in the southern part of the study area. It trends NW-SE from the Giradot sub-basin through the Eastern Cordillera to the eastern foothills over a distance of 201 km.

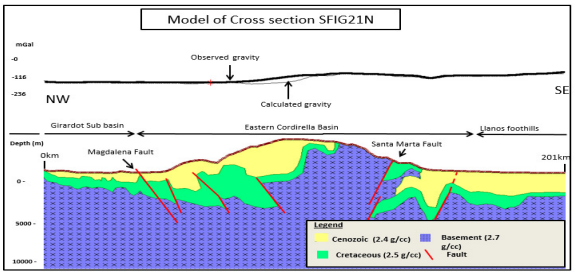

Figure 45: Final model of geologic cross section SFIG21N

After conducting all the steps described for modeling on section SFIG21N, a final model which shows a good match between the observed and calculated gravity response was obtained as shown in figure 45.

6.3 Uncertainties

Associated uncertainties in the 2D forward models are the density values which are obtained from literature due to lack of access to any available density data wells from the study area. Secondly, MT lines tend to be non-unique in the correspondence of resistivity values to lithologic units. Although, the geologic cross sections used were product of field geologic mapping as well as seismic sections, they are not a true representation of the sub-surface geology especially the deep-seated structures. Two depth seismic sections were obtained in a cartoon interpreted format which makes it difficult to make a secondary interpretation. Another uncertainty is the values used for velocity modeling which were also obtained from literature due to lack of access to any well data from the study area. The main constraint to reduce uncertainties in the development of the model is the digitized gravity data.

6.4 Summary of 2D modelling results

2D forward modeling was conducted on 20 seismic sections, 5 cross sections and 3 magnetotelluric lines. Seismic sections tend to be more reliable and require little adjustment to fit the gravity response. Magnetotelluric lines tend to fit the observed gravity almost exactly but require information from an adjacent cross section or seismic line coupled with surface geology map. The cross sections used are product of seismic lines and field mappings obtained from literature. They undergo modification especially on the Top basement. All modifications done to each model is constrained to the observed digitized gravity data and are therefore realistic.

6.5 Horizon mapping

After the models were completed, depth surfaces were generated for further analysis. Horizon maps of the Top Basement, Top Cretaceous and Top Cenozoic were generated.

6.6 Horizon mapping Procedure

The 2D forward models were used to generate depth surfaces of Top Cenozoic, Top Cretaceous and Top Basement. Points from each of these surfaces were exported and gridded to generate surface maps at an extrapolation of 10 km. The extrapolation is constrained by the gravity data as well as the Shuttle Radar Topography Mission (SRTM) elevation data.

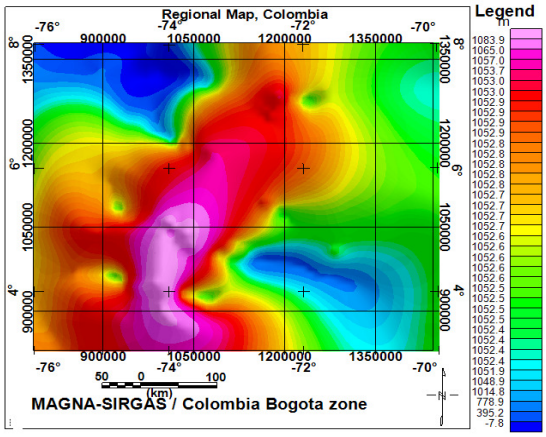

Figure 46: Top Cenozoic depth horizon map

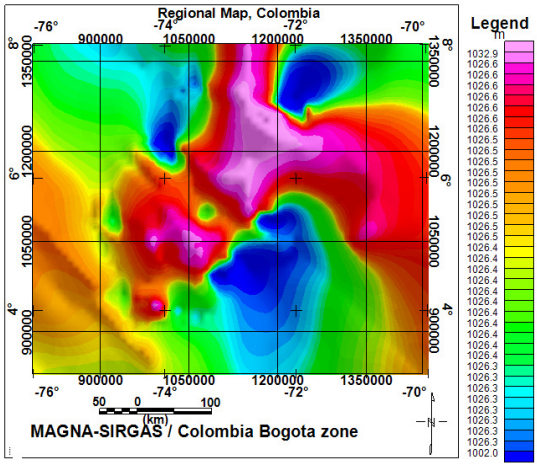

Figure 47: Top Cretaceous depth horizon map

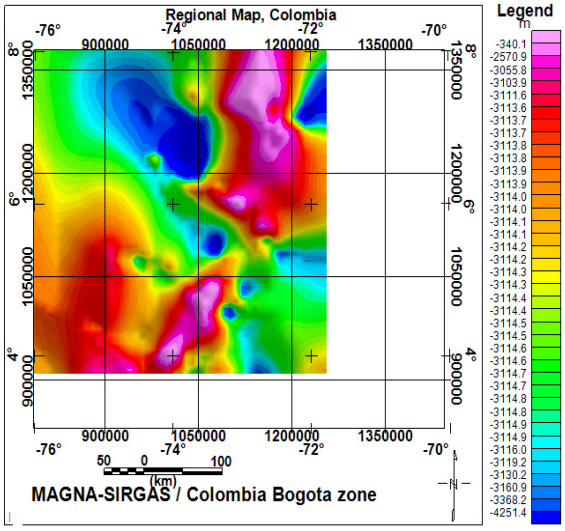

Figure 48: Top basement depth horizon map

7.0 3D Gravity Inversion

The horizon maps obtained through 2D forward modeling were used to create a 3D model. The horizons used for the 3D gravity inversion model includes the Top Moho, Top basement, Top Cretaceous and Top Cenozoic. Density values used in table 4 for

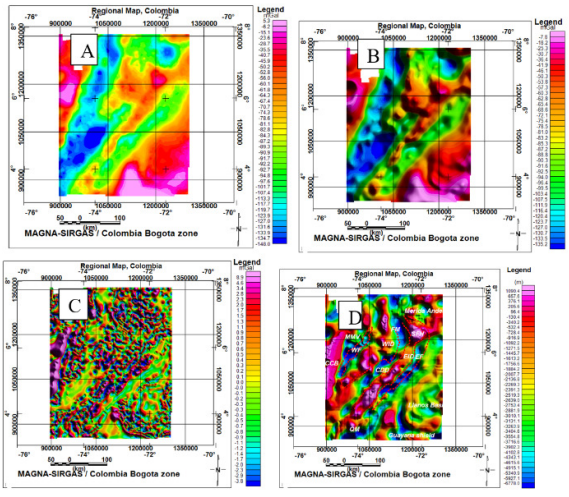

Figure 49: Panel "A" observed gravity data, "B" forward calculated model, "C" error map between "A" and "B" and "D" basement gravity response obtained from the calculated model at a wavelength of <100 km >80 km overlain with structural domains. WF = Western Foothill, WID = Western Inverted Domain, EID = Eastern Inverted Domain, CDD = Central Depressional Domain, QM = Quetame Massif, SHF = Santander Floresta High, FM = Floresta Massif, MMV = Middle Magdalena Valley, CCB = Central Cordillera Basin

the 2D model were applied to obtain the model. A simulation was run to generate the model using digitized gravity model (figure 49 A) as an observed model. A forward calculated 3D model (figure 49 B) was generated alongside an error map showing the difference between the observed model and the calculated model. In order to obtain a sediment thickness from the Shuttle Radar

The horizon maps obtained through 2D forward modeling were used to create a 3D model. The horizons used for the 3D gravity inversion model includes the Top Moho, Top basement, Top Cretaceous and Top Cenozoic. Density values used in table 4 for the 2D model were applied to obtain the model. A simulation was run to generate the model using digitized gravity model (figure 49A) as an observed model. A forward calculated 3D model (figure 49B) was generated alongside an error map showing the difference between the observed model and the calculated model. In order to obtain a sediment thickness from the Shuttle Radar Topographic Mission (SRTM) altitude map and the basement surface, the calculated model was iterated at wavelengths of >80 km but <100 km. The error map as shown in figure 49C represents the total difference between the calculated and forward models and as such, only small percentage is attributed to the basement surface map obtained. Moreover, the basement map shows a very strong correlation with the structural domain map as shown in figure 49D. A sediment thickness map was generated between the SRTM and the Top basement (figure 50A). Structural domains within the basin have been reinterpreted and a newstructural map was also obtained (figure 51D). The sediment isopach map is used to show the final prospectivity map of the Eastern Cordillera (Figure 52).

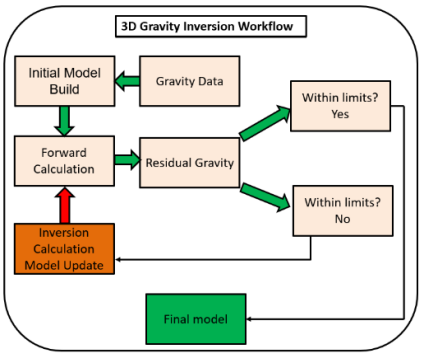

Figure 50: Work flow of 3D inversion model showing a summary of the procedures conducted in obtaining the model.

Topographic Mission (SRTM) altitude map and the basement surface, the calculated model was iterated at wavelengths of > 80 km but < 100 km. The noise map as shown in figure 49 C represents the total difference between the calculated and forward models and as such, only small percentage is attributed to the basement surface map obtained. Moreover, the basement map shows a very strong correlation with the structural domain map as shown in figure 49 D. A sediment thickness map was generated between the SRTM and the Top basement (figure 50 A). Structural domains within the basin have been reinterpreted and a new structural map was also obtained (figure 50 D).
The sediment isopach map is used to show the final prospectivity map of the Eastern Cordillera

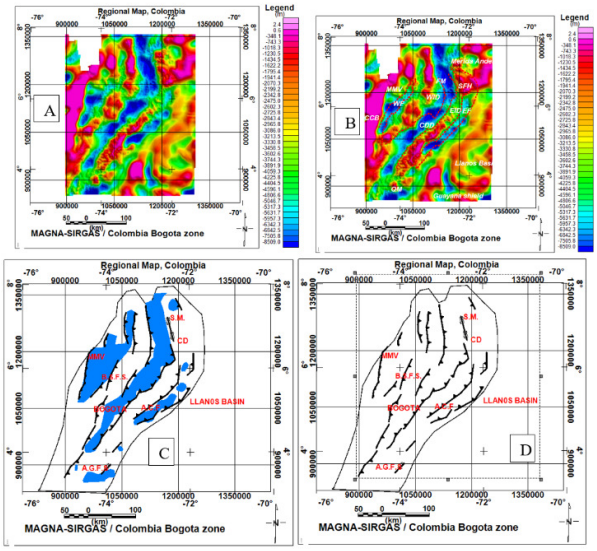

Figure 51: Panel A shows the thickness map of Eastern Cordillera derived from the 3D inversion model. Panel B shows literature structural domain on the isopach map while C shows the three areas with thickness greater than 6,500 m (blue). Panel D shows structural map derived from the isopach map. WF = Western Foothills, WID = Western Inverted Domain, EID = Eastern Inverted Domain, CDD = Central Depressional Domain, QM = Quetame Massif, SHF = Santander Floresta High, FM = Floresta Massif, MMV = Middle Magdalena Valley, CCB = Central Cordillera Basin.

8.0 Hydrocarbon Prospectivity

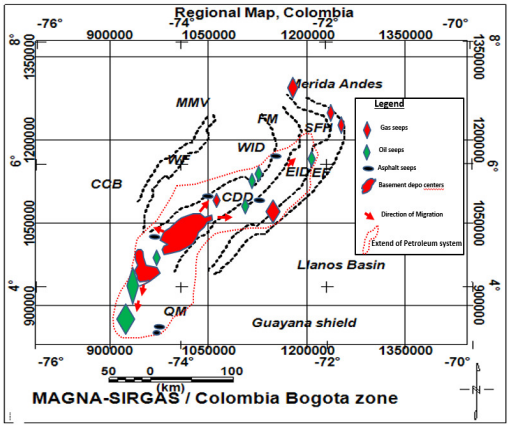

Figure 52: Petroleum system map. WF = Western Foothills, WID = Western Inverted Domain, EID = Eastern Inverted Domain, CDD = Central Depressional Domain, QM = Quetame Massif, SHF = Santander Floresta High, FM = Floresta Massif, MMV = Middle Magdalena Valley, CCB = Central Cordillera Basin. modified from Sarmiento, (2011)

The petroleum system map shows that the Bogota depression in the southern half of the Central depression Domain (CDD) generates the hydrocarbon in the basin. Migration of hydrocarbon extends to all parts of the basin with oil, gas and asphalt seeps seen mostly in the CDD and some in the Eastern Inverted and Foothills Domains

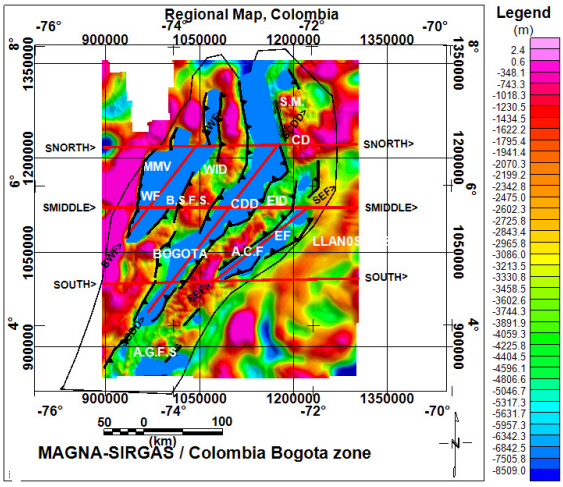

Figure 53: Prospectivity map of Eastern Cordillera showing the three main sediment rich domains (blue). Red lines show location of gravity profiles cross sections. WF = Western Foothills, WID = Western Inverted Domain, EID = Eastern Inverted Domain, CDD = Central Depressional Domain, QM = Quetame Massif, SHF = Santander Floresta High, FM = Floresta Massif, MMV = Middle Magdalena Valley, CCB = Central Cordillera Basin.

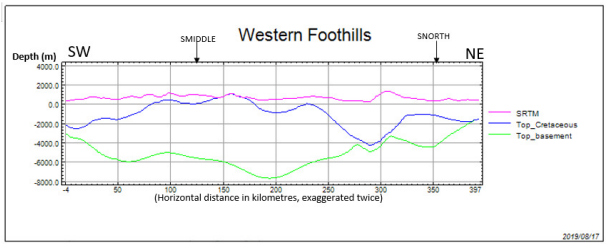

Figure 54: Cross section of gravity profile of line SWF.

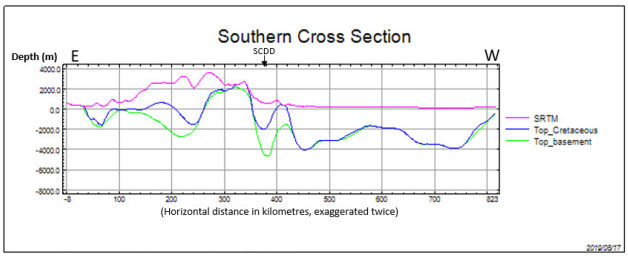

Figure 55: Cross section of gravity profile of line SOUTH.

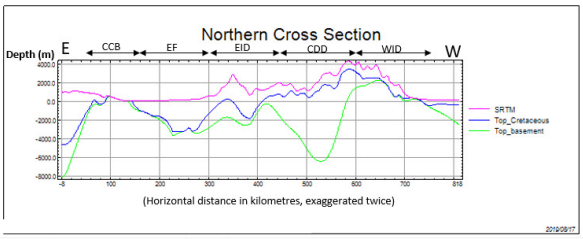

Figure 56: Cross section of gravity profile of line SNORTH. See location on figure 53. WF - Western Foothills, WID - Western Inverted Domain, EID - Eastern Inverted Domain, CDD - Central Depressional Domain, CCB – Central Cordillera Basin

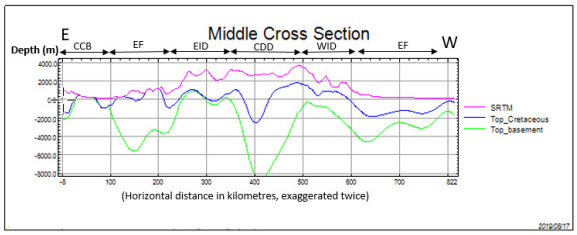

Figure 57: Cross section of gravity profile of line SMIDDLE. See location on figure 53. WF = Western Foothills, WID = Western Inverted Domain, EID = Eastern Inverted Domain, CDD = Central Depressional Domain, CCB = Central Cordillera Basin

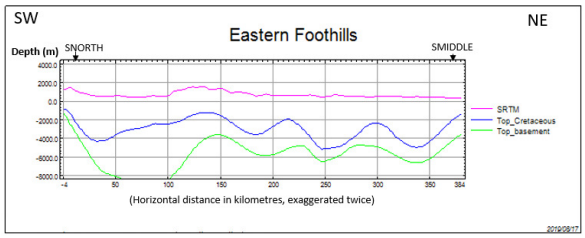

Figure 58: Cross section of gravity profile of line SEF.

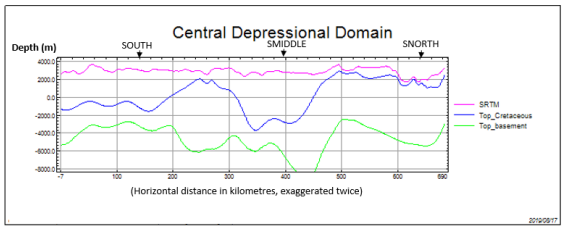

Figure 59: Cross section of gravity profile of line SCDD.

9. Discussion

Qualitative analysis has helped in identifying the five structural domains in the Eastern Cordillera which are the Central Depressional Domain (CDD), the Western Foothills (WF), the Eastern foothills (EF), and the Eastern and Western Inverted domains (EID and WID). A dominant NE – SW structural trend have been identified. Quantitative analysis has indicated that the thickest sedimentary sequences are found within the Central Depressional domain, the Western Foothills and the Eastern Foothills. 3D gravity inversion model has shown that the basement in the three domains can be as deep as 8 km to 8.5 km. This range agrees with the geologic and density models carried out by Kellogg et al., (2005) who reported that the Top Basement at the center of the Eastern Cordillera ranges from 7 km to 9.5 km and the Cretaceous section maybe as thick as 8 km using an average density of 2.5 g/cc. The result also agrees with the stratigraphic measurement of the Cretaceous reported by Cardozo (1988). Gravimetric analysis by Sarmiento (2011) also reported a sediment thickness of 5 km to 8 km on top of the Paleozoic basement. Gravity profiles across and along the three domains have indicated the potentials of both four-way and three-way dip closures (figures 53 -59).

10. Conclusion and Recommendations

1) 10.1 Conclusion

A working petroleum system has been established in the Eastern Cordillera especially now that two producer wells have been declared by the ANH in 2011 (Sarmiento, 2011). The main challenge in the region however is that of trap and timing of migration. The Cenozoic inversion may have affected the integrity of seal over the Western and Eastern Inverted Domains as most part of the Cretaceous over the areas have been exhumed and eroded. The Eastern Foothills, Western Foothills and the Central Depressional Domain contain sediment thickness of 5 km to 8.5 km as indicated by the 3D gravity inversion profiles. Gravity profiles along these domains also indicated the presence of four – way dip closures in addition to three – way dip closures against thrust mapped in the structural analysis. Repsol – YPF et al., 2002 (cited in Sarmiento, 2011) also reported the presence of these traps in the Central Depressional Domain with *breach of structures and charge* being the major associated risk factor. With the declaration of the two producer wells, it is evident that there is potential of finding prospects that satisfy a working petroleum system. The complex tectonic history of the basin may have led to formation and destruction of traps which will require detailed exploration activities to understand individual prospects within the three domains identified.

2) 10.2 Recommendations

To further understand the structural traps for exploration purposes, a modern seismic data should be acquired over the Central Depressional Domain and the Eastern and Western Foothills. However, seismic data over a fold and thrust belt can rarely be of good quality, therefore, it should be complemented with high resolution gravity data and magnetotelluric data to constrain uncertainties. Information from existing wells within these domains will be necessary for further studies. Detailed field study of potentials structures will be necessary.

11. Reference

Barrero, D., Pardo, A. and Martinez, J., 2007, Colombian Sedimentary Basins: Nomenclature, Boundaries and Petroleum Geology, a New Proposal. Agencia Nacional de Hidrocarburos. Bogotá (ANH).

Barton P. J.1986, The relationship between seismic velocity and density in the continental crust - a useful constraint? *Geophys. J. R. astr. SOC.* (1986) 87,195-208.

Burke, K., C. Cooper, J. F. Dewey, P. Mann, and J. Pindell, 1984, Caribbean tectonics and relative plate motions in the Caribbean–South American plate boundary and regional tectonics: Geological Society of America Memoir 162, p. 31–64.

Campbell, C.J., 1962. A section through the Cordillera Oriental of Colombia between Bogota and Villavicencio: 4th Annual Field Conference of the Colombian Society of Petroleum Geologists and Geophysicists, pp. 89 to 118.

Cediel, F., Shaw, R.P., and Caceres, C., 2003, Tectonic assembly of the Northern Andean Block, in C. Bartolini, R. T. Buffler, and J. Blickwede, eds., The Circum-Gulf of Mexico and the Caribbean: Hydrocarbon habitats, basin formation, and plate tectonics.: AAPG Memoir 79, p. 815–848.

Colleta, B., Hebrard, F., Letouzey, J., Werner, P., and Rudkiewicz, J.L., 1990, Tectonic style and crustal structure of the eastern cordillera (Colombia) from a balanced cross-section, in J. Letouzey, ed., Petroleum and tectonics in mobile belts: proceedings of the 4th IFP Exploration and Production Research Conference., in Technip, E., ed.: Paris, p. 81-100.

Cooper, M. A., et al., 1995, Basin development and tectonic history of the Llanos Basin, Eastern Cordillera and

Middle Magdalena Valley, Colombia: AAPG Bulletin, v. 79, p. 1421–1443.

Dengo, C. A., and M. C. Covey, 1993, Structure of the Eastern Cordillera of Colombia: Implications for trap styles and regional tectonics: AAPG Bulletin, v. 77, p. 1315–1337

Egbue, O., and Kellogg, J., 2012, Three-dimensional structural evolution and kinematics of the Piedemonte Llanero, Central Llanos foothills, Eastern Cordillera, Colombia, Journal of South American Earth Sciences, doi:10.1016

Graterol, V., and Carson-Aerogravity, 2009, La Cordillera Oriental Sector de Soapaga y e Piedemonte de La Cordillera Oriental - Llanos Orientales, Colombia., Carson Aerogravity Report.

Gregory-Wodzicki M., 2000. Uplift history of the Central and Northern Andes: A review Lamont-Doherty Earth Observatory, Columbia University, Palisades, New York 10964-8000, USA

Gregory-Wodzicki, K.M., 2000. Andean paleoelevation estimates: a review and critique. GSA Bulletin 112, 1091e1105.

Haq, B.U., Hardenbol, J. and Vail, P.R., 1987. Chronology of fluctuating sea levels since the Triassic. Science 235, 1156e1166.

Kellogg, J.N., Ojeda, G.Y., Duque, H., and Ceron, J., 2005, Crustal structure of the Eastern Cordillera, Colombia: 6th International Symposium on Andean Geodynamics (ISAG 2005): Barcelona, p. 424-427.

Linares, R., H., Alzate, J., Galindo, P., 2009, New insights into the Piedemonte license triangle zone in the Llanos foothills- Colombia.

McKenzie, D., 1978, Some remarks on the development of sedimentary basins: Earth and Planetary Science Letters, v. 40, p. 25–32.

Mejia, and V. A. Valencia, 2013, Relationship of Mesozoic graben development, stress, shortening magnitude, and structural style in the eastern Cordillera of the Colombian Andes.

Mora, A., B. Horton, A. Mesa, J. Rubiano, R. A. Ketcham, M. Parra, V. Blanco, D. Garcia, and D. Stockli, 2010, Migration of Cenozoic deformation in the Eastern Cordillera of Colombia interpreted from fission track results and structural relationships: Implications for petroleum systems: AAPG Bulletin, v. 94, no. 10, p. 1543–1580, doi:101306/01051009111

Mora, A., Parra, M.P., Strecker, M.R., Kammer, A., Dimate, C., and Rodriguez, C., 2006, Cenozoic contractional reactivation of Mesozoic extensional structures in the Eastern Cordillera of Colombia: Tectonics, v. 25.TC2010, doi:10.1029/2005TC001854

Ojeda, G., 1996. Present day retro-deformed structure of the Eastern Cordillera Cretaceous Basin, Colombia: M.Sc. thesis. University of South Carolina, 57 pp

Palacky, G. 1987, Resistivity Characteristics of Geological Targets: Electromagnetic Methods in Applied Geophysics-Theory, Society of Exploration Geophysicists Tulsa, OK, 53-129.

Pindell, J. L., and K. D. Tabbutt, 1995, Mesozoic–Cenozoic Andean paleogeography and regional controls on hydrocarbon systems, in A. J. Tankard, R. Suarez-Soruco, and H. J. Welsink, eds., Petroleum basins of South America: AAPG Memoir 62, p. 101–128.

Sarmiento-Rojas, L.F., 2001, Mesozoic rifting and Cenozoic basin inversion history of the Eastern Cordillera, Colombian Andes. Inferences from tectonic models.: Amsterdam, Ph.D. Thesis, Vrije Universiteit, p. 297, 319

Sarmiento, L. F., 2002, Mesozoic rifting and Cenozoic basin inversion of the Eastern Cordillera, Colombian Andes: Inferences from tectonic models: Ph.D. thesis, Vrije Universiteit, Amsterdam, 295 p.

Sarmiento-Rojas, L.F., Van Wess, J.D., Cloetingh, S., 2006. Mesozoic transtensional basin history of the Eastern Cordillera, Colombian Andes: inferences from tectonic models. Journal of South American Earth Sciences 21, 383e411

Sarmiento L. F., 2011. Geology and hydrocarbon potential Eastern Cordillera. Fondo editorial Universidad eafit. Vol. 7.

Sharma, P.V. 1986, Geophysical Methods in Geology. 2nd Edition, Elsevier, Amsterdam.

Taboada, A., L. A. Rivera, A. Fuenzalida, A. Cisternas, H. Philip, H. Bijwaard, J. Olaya, and C. Rivera, 2000, Geodynamics of the Northern Andes: Subduction and intracontinental deformation (Colombia): Tectonics, v. 19, no. 5, p. 787–813.

Teixell, A., Teson E., Ruiz J., and Mora A., 2015, The structure of an inverted back-arc rift: Insights from a transect across the Eastern Cordillera of Colombia near Bogota, *in* C. Bartolini and P. Mann, eds., Petroleum geology and potential of the Colombian Caribbean Margin: AAPG Memoir 108, p. 499–516.

Teson, E., Mora, A, Silva, A., Namson, J, Kammer, A., Julivert, A., Teixell, A., Castellanos, J., Casallas, W., Nemcok, M., Tamara, J., Velasquez, A., 2011, Shortening budgets in the distal parts of arc-continent collision zones: The Eastern Cordillera foreland fold and thrust belt – a view from the Northern Andes. Neotonics of Arc-Continent Collision Manizales, Colombia. A GSA

Penrose Meeting. January 17-21 2011. The Geological Society of America. Manizales. P. 34.

Toro, J., F. Roure, N. Bordas-Le Floch, S. Le Cornec-Lance, and W. Sassi, 2004, Thermal and kinematic evolution of the Eastern Cordillera fold and thrust belt, Colombia, in R. Swennen, F. Roure, and J. W. Granath, eds., Deformation, fluid flow, and reservoir appraisal in foreland fold and thrust belts: AAPG Hedberg Series, no. 1, p. 79– 115.

Trenkamp, R., Kellogg, J.N., Freymuller, J.T., Mora, H.P., 2002. Wide plate margin deformation, South Central America and Northwestern South America, CASA GPS observations. Journal of South American Earth Sciences 15, 157e171.

Veiga R. and Dzelalija F., 2014. A Regional Overview of the La Luna Formation and the Villeta Group as Shale Gas/Shale Oil in the Catatumbo, Magdalena Valley and Eastern Cordillera Regions, Colombia. Adapted from extended abstract prepared for oral presentation at AAPG International Conference & Exhibition, Cartagena, Colombia.

Villamil, T., 1999, Campanian–Miocene tectonostratigraphy, depocenter evolution and basin development of Colombia and western Venezuela: Palaeogeography, Palaeoclimatology, Palaeoecology, v. 153, no. 4, p. 239–275, doi:10.1016/S0031-0182(99)00075-9

Villamil, T., Kauffman, E.G., Mar 1993. Milankovitch climate cyclicity and its effect on relative sea level changes and organic carbon storage, Late Cretaceous black shales of Colombia and Venezuela. In: International Congress of the American Association of Petroleum Geologists, Caracas (Venezuela), pp. 14e17.

Wortel, R., 1984. Spatial and temporal variations in the Andean subduction zone. Journal of the Geological Society 141, 783e791

